TABLE OF CONTENTS

TABLE OF CONTENTS
(continued)

TABLE OF CONTENTS
(continued)

TABLE OF CONTENTS
(continued)

TABLE OF CONTENTS
(continued)

6.0 RACK STRUCTURAL CONSIDERATIONS

The purpose of this section is to demonstrate the structural adequacy of the James A. FitzPatrick Plant spent fuel rack design under normal and accident loading conditions following the guidelines of the USNRC OT Position Paper (Ref. 6.12). The method of analysis presented uses a time-history integration method similar to that previously used in the licensing reports on high density spent fuel racks for Fermi 2 (USNRC Docket No. 50-341), Quad Cities 1 and 2 (USNRC Docket Nos. 50-254 and 50-265), Rancho Seco (USNRC Docket No. 50-312), Grand Gulf Unit 1 (USNRC Docket No. 50-416), Oyster Creek (USNRC Docket No. 50-219), V.C. Summer (USNRC Docket No. 50-395), Diablo Canyon Units 1 and 2 (USNRC Docket Nos. 50-275 and 50-323), Vogtle Unit 2 (USNRC Docket No. 50-425) and Millstone Point Unit 1 (USNRC Docket No. 50-245). The results show that the high density spent fuel racks are structurally adequate to resist the postulated stress combinations associated with level A, B, C, and D conditions as defined in References 6-1 and 6-2.

6.1 ANALYSIS OUTLINE (FOR NEW PROPOSED RACK MODULES)

The spent fuel storage racks are Seismic Class I equipment. They are required to remain functional during and after a Safe Shutdown Earthquake (Ref. 6-3). As noted previously, these racks are neither anchored to the pool floor nor attached to the sidewalls. The individual rack modules are not interconnected. Furthermore, a particular rack may be completely loaded with fuel

assemblies (which corresponds to greatest rack inertia), or it may be completely empty. The coefficient of friction, μ, between the supports and pool floor is another indeterminate factor. According to Rabinowicz (Ref. 6-4), the results of 199 tests performed on austenitic stainless steel plates submerged in water show a mean value of μ to be 0.503 with a standard deviation of 0.125. The upper and lower bounds (based on twice the standard deviation) are thus 0.753 and 0.253, respectively. Analyses are performed for single rack simulations assemblies with values of the coefficient of friction equal to 0.2 (lower limit) and 0.8 (upper limit), respectively. In order to predict the limiting conditions of rack module seismic response, the rack module with the maximum aspect ratio (length to width ratio), and maximum mass inertia should be evaluated. Therefore, the 6x14 and 11x12 modules merit seismic simulation for critical conditions of loading. They are:

- Fully loaded rack (all storage locations occupied), μ = 0.8; 0.2 (μ = coefficient of friction)
- Nearly empty rack (6x14 only)

The simulations were performed using normal (unconsolidated) fuel; simulations are also performed for a heavier fuel. These modules are labelled Modules B and C in Section 2. As stated before, the former was selected due to its largest mass inertia, and the latter due to its maximum aspect ratio. 2-D multi-rack analyses are also performed to examine the interaction between racks.

The seismic analyses were performed utilizing the time-history method. Pool slab acceleration data in three orthogonal directions was developed and verified to be statistically independent.

The objective of the seismic analysis of single racks is to determine the structural response (stresses, deformation, rigid body motion, etc.) due to simultaneous application of the three statistically independent, orthogonal seismic excitations. Thus, recourse to approximate statistical summation techniques such as the "Square-Root-of-the-Sum-of-the-Squares" method (Ref. 6-5) is avoided. For nonlinear analysis, the only practical method is simultaneous application of the seismic loading to a nonlinear model of the structure.

Pool slab acceleration data are developed from specified response spectra from two earthquakes: SSE and OBE. Seismic time histories are calculated from the plant response spectra at level 326.8' at 1% damping. Figures 6.1 - 6.12 show the time-histories and comparison of the corresponding velocity spectra and the design spectra for SSE and OBE conditions.

The seismic analysis of a single rack is performed in three steps, namely:

1. Development of a nonlinear dynamic model consisting of inertial mass elements, spring, gap, and friction elements.

2. Generation of the equations of motion and inertial coupling and solution of the equations using the "component element time integration scheme" (References 6-6 and 6-7) to determine nodal forces and displacements.

3. Computation of the detailed stress field in the rack just above the baseplate and in the support legs using the nodal forces calculated in the previous step. These stresses are checked against the design limits given in Section 6.5.

A brief description of the dynamic model follows.

6.2 FUEL RACK - DYNAMIC MODEL

Since the racks are not anchored to the pool slab or attached to the pool walls or to each other, they can execute a wide variety of motions. For example, the rack may slide on the pool floor (so-called "sliding condition"); one or more legs may momentarily lose contact with the liner ("tipping condition"); or the rack may experience a combination of sliding and tipping conditions. The structural model should permit simulation of these kinematic events with inherent built-in conservatisms. Since the modules are designed to preclude the incidence of inter-rack impact, it is also necessary to include the potential for inter-rack impact phenomena in the analysis to demonstrate that such impacts do not occur. Lift off of the support legs and subsequent liner impacts must be modelled using appropriate impact (gap) elements, and Coulomb friction between the rack and the pool liner must be simulated by appropriate piecewise linear springs. The elasticity of the rack structure, relative to the base, must also be included in the model even though the rack may be nearly rigid. These special attributes of the rack dynamics require a strong emphasis on the modeling of the linear and nonlinear springs, dampers, and compression only stop elements. The term non-linear spring is the generic term to denote the mathematical element representing the situation where the restoring force exerted by the element is not linearly proportional to the displacement. In the fuel rack simulation the Columb friction interface between the rack support leg and the liner is a typical example of a non-linear spring. The model outline in the remainder of this section, and the model description in the following

section, describe the detailed modeling technique to simulate these effects, with emphasis placed on the nonlinearity of the rack seismic response.

6.2.1 Outline of Model for Computer Code DYNARACK

a. The fuel rack structure is a folded metal plate assemblage welded to a baseplate and supported on four legs. An odd-shaped module may have more than four legs. The rack structure itself is a very rigid structure. Dynamic analysis of typical multicell racks has shown that the motion of the structure is captured almost completely by modelling the rack as a twelve degree-of-freedom structure, where the movement of the rack cross-section at any height is described in terms of six degrees-of-freedom of the rack base and six degrees of freedom defined at the rack top. The rattling fuel is modelled by five lumped masses located at H, .75H, .5H, .25H, and at the rack base, where H is the rack height as measured from the base.

b. The seismic motion of a fuel rack is characterized by random rattling of fuel assemblies in their individual storage locations. Assuming a certain statistical coherence (i.e. assuming that all fuel elements move in-phase within a rack) in the vibration of the fuel assemblies exaggerates the computed dynamic loading on the rack structure. This assumption, however, greatly reduces the required degrees-of-freedom needed to model the fuel assemblies which are represented by five lumped masses located at different levels of the rack. The centroid of each fuel assembly mass can be located, relative to the rack structure centroid at that level, so as to simulate a partially loaded rack.

c. The local flexibility of the pedestal is modelled so as to account for floor elasticity, and local rack elasticity just above the pedestal.

d. The rack base support may slide or lift off pool floor.

e. The pool floor has a specified time-hi of seismic accelerations along the three orthogonal dir ons.

f. Fluid coupling between rack and fuel assemblies, and between rack and adjacent racks, is simulated by introducing appropriate inertial coupling into the system kinetic energy. Inclusion of these effects uses the methods of References 6-4 and 6-6 for rack/assembly coupling and for rack/rack coupling (see Section 6.2.3 of this report).

g. Potential impacts between rack and fuel assemblies are accounted for by appropriate "compression only" gap elements between masses involved.

h. Fluid damping due to viscous effects between rack and assemblies, and between rack and adjacent rack, is conservatively neglected; form drag, however, may be included.

i. The supports are modeled as "compression only" elements for the vertical direction and as "rigid links" for transferring horizontal stress. The bottom of a support leg is attached to a frictional spring as described in Section 6.3. The cross-section inertial properties of the support legs are computed and used in the final computations to determine support leg stresses.

j. The effect of sloshing is negligible at the level of the top of the rack and is hence neglected.

k. The possible incidence of inter-rack impact is simulated by gap elements at the top and bottom of the rack in the two horizontal directions. The most conservative case of adjacent rack movement is assumed; each adjacent rack is assumed to move completely out of phase with the rack being analyzed. This maximizes the potential for impact.

l. Rattling of fuel assemblies inside the storage locations causes the "gap" between the fuel assemblies and the cell wall to change from a maximum of twice the nominal gap to a theoretical zero gap. Fluid coupling coefficients are based on the nominal gap.

m. The cross coupling effects due to the movement of fluid from one interstitial (inter-rack) space to the adjacent one is modelled using potential flow and Kelvin's circulation theorem. This formulation has been reviewed and approved by the Nuclear Regulatory Commission, during the post-licensing multi-rack analysis for Diablo Canyon Unit I and II reracking project. The coupling coefficients are based on a consistent modelling of the fluid flow. While updating of the fluid flow coefficients, based on the current gap, is permitted in the algorithm, the analyses here are conservatively carried out using the constant nominal gaps that exist at the start of the event.

Figure 6.13 shows a schematic of the model. Twelve degrees of freedom are used to track the motion of the rack structure. Figures 6.14 and 6.15, respectively, show the inter-rack impact springs (to track the potential for impact between racks) and fuel assembly/storage cell impact springs at a particular level.

As shown in Figure 6.13, the model for simulating fuel assembly motion incorporates five rattling lumped masses. The five rattling masses are located at the baseplate, at quarter height, at half height, at three quarter height, and at the top of the rack. Two degrees of freedom are used to track the motion of each rattling mass in the horizontal plane. The vertical motion of each rattling mass is assumed to be the same as the rack base. Figures 6.16, 6.17 and 6.18 show the modelling scheme for including rack elasticity and the degrees of freedom associated with rack elasticity. In each plane of bending a shear and a bending spring are used to simulate elastic effects in accordance with Reference 6.6. Table 6.3 gives spring constants for these bending springs as well as corresponding constants for extensional and torsional rack elasticity.

6.2.2 Model Description

The absolute degrees of freedom associated with each of the mass locations are identified in Figure 6.13 and in Table 6.1. The rattling masses (nodes 1^*, 2^*, 3^*, 4^*, 5^*) are described by translational degrees-of-freedom q_7-q_{16}.

$U_i(t)$ is the pool floor slab displacement seismic time-history. Thus, there are twenty-two degrees of freedom in the system. Not shown in Fig. 6.13 are the gap elements used to model the support legs and the impacts with adjacent racks.

6.2.3 Fluid Coupling

An effect of some significance requiring careful modeling is the "fluid coupling effect". If one body of mass (m_1) vibrates adjacent to another body (mass m_2), and both bodies are submerged in a frictionless fluid medium, then Newton's equations of motion for the two bodies have the form:

$$(m_1 + M_{11})\ddot{X}_1 + M_{12}\ddot{X}_2 = \text{applied forces on mass } m_1 + O(\dot{x}_1^2)$$

$$+M_{21}\ddot{X}_1 + (m_2 + M_{22})\ddot{X}_2 = \text{applied forces on mass } m_2 + O(\dot{x}_2^2)$$

$\ddot{X}_1$, $\ddot{X}_2$ denote absolute accelerations of mass m_1 and m_2, respectively.

M_{11}, M_{12}, M_{21}, and M_{22} are fluid coupling coefficients which depend on the shape of the two bodies, their relative disposition, etc. Fritz (Ref. 6-9) gives data for M_{ij} for various body shapes and arrangements. The above equation indicates that the effect of the fluid is to add a certain amount of mass to the body (M_{11} to body 1), and an external force which is proportional to the

acceleration of the adjacent body (mass m_2). Thus, the acceleration of one body affects the force field on another. This force is a strong function of the interbody gap, reaching large values for very small gaps. This inertial coupling is called fluid coupling. It has an important effect in rack dynamics. The lateral motion of a fuel assembly inside the storage location will encounter this effect. So will the motion of a rack adjacent to another rack. These effects are included in the equations of motion. For example, the fluid coupling is between nodes 2 and 2* in Figure 6.13. Furthermore, the rack equations contain coupling terms which model the effect of fluid in the gaps between adjacent racks. The coupling terms modeling the effects of fluid flowing between adjacent racks are computed assuming that all adjacent racks are vibrating 180^0 out of phase from the rack being analyzed. Therefore, only one rack is considered surrounded by a hydrodynamic mass computed as if there were a plane of symmetry located in the middle of the gap region.

The rack-to-rack hydrodynamic mass coupling coefficients M_{ij} are inversely proportional to the annular gap between the two bodies. This gap is a function of time as the two bodies vibrate, so that the hydrodynamic coefficients M_{ij} are functions of time as well. In the previous equations, the notation $O(\dot{x}_1^2)$, $O(\dot{x}_2^2)$ represent additional nonlinear fluid restoring forces that arise from the development of the interbody fluid coupling effects. These nonlinear restoring forces are only important as the gaps between bodies become small as they are also proportional to the inverse of the square of the current gap. Proper accounting of the effect of gap size on the hydrodynamic mass M_{ij} and on the

fluid restoring forces due to film squeezing is permitted at each step in the dynamic simulation. If the hydrodynamic mass is conservatively based on the nominal gap, and no updating is included, then these additional geometric nonlinear terms are not present.

Finally, fluid virtual mass is included in the vertical direction vibration equations of the rack; virtual inertia is also added to the governing equation corresponding to the rotational degree of freedom, $q_6(t)$ and $q_{22}(t)$.

6.2.4 Damping

In reality, damping of the rack motion arises from material hysteresis (material damping), relative intercomponent motion in structures (structural damping), and fluid viscous effects (fluid damping). In the analysis, a maximum of 1% structural damping is imposed on elements of the rack structure during OBE seismic simulations and 2% for SSE simulation. Material and fluid damping due to fluid viscosity are conservatively neglected. The dynamic model has the provision to incorporate form drag effects; however, no form drag has been used for this analysis. Subsequent to the completion of all dynamic runs which are reported in Tables 6.5 and 6.6, key (governing) cases were rerun with 1% damping for both OBE and SSE simulations per FSAR requirements. The results show a very minor increase in the equipment response, and all required stress and displacement limits are satisfied.

6.2.5 Impact

Any fuel assembly node (e.g., 2*) may impact the corresponding structural mass node 2. To simulate this impact, four compression-only gap elements around each rattling fuel assembly node are provided (see Figure 6.15). The compressive loads developed in these springs provide the necessary data to evaluate the integrity of the cell wall structure and stored array during the seismic event. Figure 6.14 shows the location of the

impact springs used to simulate any potential for inter-rack impacts. Section 6.4.2 gives more details on these additional impact springs. Since there are five rattling masses, a total of 20 impact springs are used to model fuel assembly-cell wall impact.

6.3 ASSEMBLY OF THE DYNAMIC MODEL

The cartesian coordinate system associated with the rack has the following nomenclature:

- x = Horizontal coordinate along the short direction of rack rectangular platform
- y = Horizontal coordinate along the long direction of the rack rectangular platform
- z = Vertical coordinate upward from the rack base

If the simulation model is restricted to two dimensions (one horizontal motion plus vertical motion, for example) for the purposes of model clarification only, then a descriptive model of the simulated structure which includes gap and friction elements is shown in Figure 6.19.

The impacts between fuel assemblies and rack show up in the gap elements, having local stiffness K_I, in Figure 6.13. In Table 6.2, gap elements 5 through 8 are for the vibrating mass at the top of the rack. The support leg spring rates K_S are modeled by elements 1 through 4 in Table 6.2. Note that the local compliance of the concrete floor is included in K_S. To simulate sliding potential, friction elements 2 plus 8 and 4 plus 6 (Table 6.2) are shown in Figure 6.19. The friction of the support/liner interface is modeled by a piecewise linear spring with a suitably large stiffness K_f up to the limiting lateral load, μN, where N is the

current compression load at the interface between support and liner. At every time step during the transient analysis, the current value of N (either zero for liftoff condition, or a compressive finite value) is computed. Finally, the support rotational friction springs K_R reflect any rotational restraint that may be offered by the foundation. This spring rate is calculated using a modified Bousinesq equation (Ref. 6-4) and is included to simulate the resistive moment of the support to counteract rotation of the rack leg in a vertical plane. This rotation spring is also nonlinear, with a zero spring constant value assigned after a certain limiting condition of slab moment loading is reached.

The nonlinearity of these springs (friction elements 9, 11, 13, and 15 in Table 6.2) reflects the edging limitation imposed on the base of the rack support legs and the shifts in the centroid of load application as the rack rotates. If this effect is neglected; any support leg bending, induced by liner/baseplate friction forces, is resisted by the leg acting as a beam cantilevered from the rack baseplate. This leads to higher predicted loads at the support leg - baseplate junction than if the moment resisting capacity due to floor elasticity at the floor is included in the model.

The spring rate K_S modeling the effective compression stiffness of the structure in the vicinity of the support, is computed from the equation:

$$\frac{1}{K_S} = \frac{1}{K_1} + \frac{1}{K_2} + \frac{1}{K_3}$$

where:

K_1 = spring rate of the support leg treated as a tension-compression member

K_2 = local spring rate of pool slab

K_3 = spring rate of folded plate cell structure above support leg

As described in the preceding section, the rack, along with the base, supports, and stored fuel assemblies, is modeled for the general three-dimensional (3-D) motion simulation by a twenty-two degree of freedom model. To simulate the impact and sliding phenomena expected, up to 64 nonlinear gap elements and 16 nonlinear friction elements are used. Gap and friction elements, with their connectivity and purpose, are presented in Table 6.2. Table 6.3 lists representative values for the B and C modules used in the dynamic simulations.

For the 3-D simulation of a single rack, all support elements (described in Table 6.2) are included in the model.* Coupling between the two horizontal seismic motions is provided both by any offset of the fuel assembly group centroid which causes the rotation of the entire rack and/or by the possibility of liftoff

---

* Since inter-rack impact does not occur in the subject modules, only 8 gap elements are used around the bottom and top edges of the rack instead of the twenty described in Table 6.2. Since their purpose is only to signal if an impact occurs, the exact number utilized has no bearing on the final reported results.

of one or more support legs. The potential exists for the rack to be supported on one or more support legs during any instant of a complex 3-D seismic event. All of these potential events may be simulated during a 3-D motion and have been observed in the analyses.

6.4 TIME INTEGRATION OF THE EQUATIONS OF MOTION

6.4.1 Time-History Analysis Using Multi-Degree of Freedom Rack Model

Having assembled the structural model, the dynamic equations of motion corresponding to each degree of freedom are written by using Lagrange's Formulation. The system kinetic energy can be constructed including contributions from the solid structures and from the trapped and surrounding fluid. A single rack is modelled in detail. The system of equations can be represented in matrix notation as:

$$[M]\{q''\} = \{Q\} + \{G\}$$

where the vector $\{Q\}$ is a function of nodal displacements and velocities, and $\{G\}$ depends on the coupling inertia and the ground acceleration. Premultiplying the above equations by $[M]^{-1}$ renders the resulting equation uncoupled in mass.

We have:

$$\{q''\} = [M]^{-1}\{Q\} + [M]^{-1}\{G\}$$

Note that since the mass matrix can be updated at every time step because of the time varying hydrodynamic effects, the inversion of the equations is carried out at every increment when the updating option is used. The effect of the previously mentioned nonlinear fluid restoring forces is included in the

generalized forces Q and accounted for in the analysis when the updating option is used. As noted before, the analyses performed here do not use the updating option.

As noted earlier, in the numerical simulations run to verify structural integrity during a seismic event, the rattling fuel assemblies are assumed to move in phase. This will provide maximum impact force level, and induce additional conservatism in the time-history analysis.

This equation set is mass uncoupled, displacement coupled at each instant in time, and is ideally suited for numerical solution using a central difference scheme. The proprietary, USNRC qualified, computer program "DYNARACK"* is utilized for this purpose.

Stresses in various portions of the structure are computed from known element forces at each instant of time and the maximum value of critical stresses over the entire simulation is reported in summary form at the end of each run.

---

* This code has been previously utilized in licensing of similar racks for Fermi 2 (USNRC Docket No. 50-341), Quad Cities 1 and 2 (USNRC Docket Nos. 50-254 and 265), Rancho Seco (USNRC Docket No. 50-312), Oyster Creek (USNRC Docket No. 50-219), V.C. Summer (USNRC Docket No. 50-395), and Diablo Canyon 1 and 2 (USNRC Docket Nos. 50-275 and 50-323), St. Lucie Unit I (USNRC Docket No. 50-335), Byron Units I and II (USNRC Docket Nos. 50-454, 50-455), Vogtle 2 (USNRC Docket 50-425), and Millstone Unit 1 (USNRC Docket 50-245).

In summary, dynamic analysis of typical multicell racks has shown that the motion of the structure is captured almost completely by the behavior of a twenty-two degree of freedom structure; therefore, in this analysis model, the movement of the rack cross-section at any height is described in terms of the rack degrees of freedom ($q_1(t),...q_6(t)$ and q_{17}-$q_{22}(t)$). The remaining degrees of freedom are associated with horizontal movements of the fuel assembly masses. In this dynamic model, five rattling masses are used to represent fuel assembly movement in the horizontal plane. Therefore, the final dynamic model consists of twelve degrees of freedom for the rack plus ten additional mass degrees of freedom for the five rattling masses. The totality of fuel mass is included in the simulation and is distributed among the five rattling masses.

6.4.2 Evaluation of Potential for Inter-Rack Impact

Since the racks are closely spaced, the simulation includes impact springs to model the potential for inter-rack impact. To account for this potential, yet still retain the simplicity of simulating only a single rack, gap elements are located on the rack at the top and at the baseplate level. Figure 6.14 shows the location of these gap elements. Where impacts between racks is permitted by specification, twenty gap elements at each level would be used as shown. The rack design specification precludes any impacts between racks or between rack and walls during any single event; therefore, only sixteen impact springs are retained (8 at top and 8 at baseplates) solely to demonstrate that the postulated gaps do not close completely due to rack motion.

6.5 STRUCTURAL ACCEPTANCE CRITERIA

There are two sets of criteria to be satisfied by the rack modules:

a. Kinematic Criterion

This criterion seeks to ensure that the rack is a physically stable structure. The FitzPatrick racks are designed to preclude inter-rack impacts. Therefore, physical stability of the rack is considered along with the criterion that inter-rack impact or rack-to-wall impacts do not occur.

b. Stress Limits

The stress limits of the ASME Code, Section III, Subsection NF, 1983 Edition are used since this code provides the most appropriate and consistent set of limits for various stress types and various loading conditions. The following loading combinations are applicable (Ref. 6-1) and are consistent with the plant FSAR commitments.

Loading Combination	Stress Limit
$D + L$ $D + L + T_o$ $D + L + T_o + E$	Level A service limits
$D + L + T_a + E$ $D + L + T_o + P_f$	Level B service limits
$D + L + T_a + E'$ $D + L + F_d$	Level D service limits The functional capability of the fuel racks should be demonstrated.

where:

D = Dead weight-induced stresses (including fuel assembly weight)

L = Live Load (0 for the structure, since there are no moving objects in the rack load path).

F_d = Force caused by the accidental drop of the heaviest load from the maximum possible height.

P_f = Upward force on the racks caused by postulated stuck fuel assembly

E = Operating Basis Earthquake (OBE)

E' = Safe Shutdown Earthquake (SSE)

T_o = Differential temperature induced loads (normal or upset condition)

T_a = Differential temperature induced loads (abnormal design conditions)

The conditions T_a and T_o cause local thermal stresses to be produced. The worst situation will be obtained when an isolated storage location has a fuel assembly which is generating heat at the maximum postulated rate. The surrounding storage locations are assumed to contain no fuel. The heated water makes unobstructed contact with the inside of the storage walls, thereby producing the maximum possible temperature difference between the adjacent cells. The secondary stresses thus produced are limited to the body of the rack; that is, the support legs do not experience the secondary (thermal) stresses.

6.6 MATERIAL PROPERTIES

The data on the physical properties of the rack and support materials, obtained from the ASME Boiler & Pressure Vessel Code, Section III, appendices, are listed in Table 6.4. Since the

maximum pool bulk temperature is less than 150°F, this is used as the reference design temperature for evaluation of material properties.

6.7 STRESS LIMITS FOR VARIOUS CONDITIONS

The following stress limits are derived from the guidelines of the ASME Code, Section III, Subsection NF, in conjunction with the material properties data of the preceding section.

6.7.1 Normal and Upset Conditions (Level A or Level B)

a. Allowable stress in tension on a net section $= F_t = 0.6\ S_y$ or

$F_t = (0.6)\ (23,150) = 13,890$ psi (rack material)

F_t = is equivalent to primary membrane stresses
$F_t = (.6)\ (23,150) = 13,890$ psi (upper part of support feet)

$= (.6)\ (101,040) = 60,625$ psi (lower part of support feet)

b. On the gross section, allowable stress in shear is:

$F_v = .4\ S_y$
$(.4)\ (23,150) = 9,260$ psi (main rack body)

$F_t = (.4)\ (23,150) = 9,260$ psi (upper part of support feet)

$= (.4)\ (101,040) = 40,416$ psi (lower part of support feet)

c. Allowable stress in compression, F_a:

$$F_a = \frac{\left[1 - \frac{kl^2}{r^2} / 2C_c^2\right] S_y}{\left(\frac{5}{3}\right) + \left[3\left(\frac{kl}{r}\right) / 8C_c\right] - \left[\left(\frac{kl}{r}\right)^3 / 8C_c^3\right]}$$

where:

$$C_c = \left[\frac{(2\pi^2 E)}{S_y}\right]^{1/2}$$

kl/r for the main rack body is based on the full height and cross section of the honeycomb region. Substituting numbers, we obtain, for both support leg and honeycomb region:

F_a = 13,890 psi (main rack body)
F_a = 13,890 psi (upper part of support feet)
= 60,625 psi (lower part of support feet)

d. Maximum allowable bending stress at the outermost fiber due to flexure about one plane of symmetry:

$F_b = 0.60\ S_y$ = 13,890 psi (rack body)
F_b = 13,890 psi (upper part of support feet)
= 60,625 psi (lower part of support feet)

e. Combined flexure and compression:

$$\frac{f_a}{F_a} + \frac{C_{mx}\ f_{bx}}{D_x F_{bx}} + \frac{C_{my} f_{by}}{D_y F_{by}} < 1$$

where:

f_a = Direct compressive stress in the section

f_{bx} = Maximum flexural stress along x-axis

f_{by} = Maximum flexural stress along y-axis

$C_{mx} = C_{my} = 0.85$

$$D_x = 1 - \frac{f_a}{F'_{ex}}$$

$$D_y = 1 - \frac{f_a}{F'_{ey}}$$

where:

$$F'_{ex,ey} = \frac{12\ \pi^2\ E}{23\ \left(\frac{kl_{bx,y}}{r_{bx,y}}\right)^2}$$

and the subscripts x,y reflect the particular bending plane of interest.

f. Combined flexure and compression (or tension):

$$\frac{f_a}{0.6S_y} + \frac{f_{bx}}{F_{bx}} + \frac{f_{by}}{F_{by}} < 1.0$$

The above requirement should be met for both the direct tension or compression case.

6.7.2 Level D Service Limits

F-1370 (ASME Section III, Appendix F), states that the limits for the Level D condition are the minimum of 1.2 (S_y/F_t) or ($0.7S_u/F_t$) times the corresponding limits for Level A condition. Since 1.2 S_y is greater than 0.7 S_u for the lower part of the support feet, the factor is 1.674 for the lower section under SSE conditions. The factor for the upper portion of the support foot is 2.0.

Instead of tabulating the results of these six different stresses as dimensioned values, they are presented in a dimensionless form. These so-called stress factors are defined as the ratio of the actual developed stress to its specified limiting value. With this definition, the limiting value of each stress factor is 1.0 for the OBE and 2.0 (or 1.674) for the SSE condition.

6.8 RESULTS FOR THE ANALYSIS OF SPENT FUEL RACKS USING A SINGLE RACK MODEL AND 3-D SEISMIC MOTION

A complete synopsis of the analysis of the modules subject to the postulated earthquake motions, is presented in a summary Table 6.5 which gives the bounding values of stress factors R_i (i = 1,2,3,4,5,6). The stress factors are defined as:

R_1 = Ratio of direct tensile or compressive stress on a net section to its allowable value (note support feet only support compression)

R_2 = Ratio of gross shear on a net section in the x-direction to its allowable value

R_3 = Ratio of maximum bending stress due to bending about the x-axis to its allowable value for the section

R_4 = Ratio of maximum bending stress due to bending about the y-axis to its allowable value

R_5 = Combined flexure and compressive factor (as defined in 6.7.1e above)

R_6 = Combined flexure and tension (or compression) factor (as defined in 6.7.1f above)

R_7 = Ratio of gross shear on a net section in the y-direction to its allowable value.

As stated before, the allowable value of R_i (i =1,2,3,4,5,6) is 1 for the OBE condition and 2 for the SSE (except for the lower section of the support where the factor is 1.674)

The dynamic analysis gives the maximax (maximum in time and in space) values of the stress factors at critical locations in the rack module. Values are also obtained for maximum rack displacements and for critical impact loads. Table 6.5 presents critical results for the stress factors, and rack to fuel impact load. Table 6.6 presents maximum results for horizontal displacements at the top and bottom of the rack in the x and y direction. "x" is always the short direction of the rack. In Table 6.6, for each run, both the maximum value of the sum of all support foot loadings (4 supports) as well as each individual maximum is reported. The table also gives values for the maximum vertical load and the corresponding net shear force at the liner at essentially the same time instant, and for the maximum net shear load and the corresponding vertical force at a support foot at essentially the same time instant.

The results presented in Tables 6.5, 6.6 are representative of the totality of runs carried out. The critical case for structural integrity calculations is included. Appendix A to this Section 6 contains a partial output from one of the DYNARACK simulation runs of a single rack under 3-D excitation. The initial pages showing input data and model description are given along with the final summary pages giving maximum loads, displacements, and stress factors.

The results corresponding to SSE give the highest load factors. However, the results given for the SSE still yield maximum stress factors (R_i) below the limiting value for the OBE condition for all sections.The critical load factors reported for the support feet are all for the upper segment of the foot and for SSE simulations are to be compared with the limiting value of 2.0. Results for the lower portion of the support foot are not critical and are not reported in the tables.

Analyses show that significant margins of safety exist against local deformation of the fuel storage cell due to rattling impact of fuel assemblies.

Results obtained for partially loaded racks will be enveloped by the data presented. Overturning has also been considered for the case of the C rack adjacent to an open area. This has been done by assuming a multiplier of 1.5 on the SSE horizontal earthquakes (more conservative than the OT Position Paper) and checking predicted displacements if there were no obstacles. The horizontal displacements do not grow to such an

extent as to imply any possibility for overturning. Run C03 presents the maximum displacements for the case where the horizontal excitation level is increased by 50%.

6.9 IMPACT ANALYSES

6.9.1 Impact Loading Between Fuel Assembly and Cell Wall

The local stress in a cell wall is conservatively estimated from the peak impact loads obtained from the dynamic simulations. Plastic analysis is used to obtain the limiting impact load. The limit load is calculated as 4585 lbs. per cell which is much greater than the loads obtained from any of the simulations.

6.9.2 Impacts Between Adjacent Racks

All of the dynamic analyses assume, conservatively, that adjacent racks move completely out of phase. Thus, the highest potential for inter-rack impact is achieved. The displacements obtained from the dynamic analyses are less than 50% of the rack-to-rack spacing or rack-to-wall spacing.

It is also noted that the new fuel racks do not breach the theoretical plane between the new racks and the contiguous existing racks, indicating that impact with existing rack modules will not occur. This is a plausible conclusion in view of the fact that the existing racks and new racks have markedly different structural characteristics and their displacement time histories will be randomly phased with respect to each other.

Therefore, we conclude that no impacts between racks or between racks and walls occur during the SSE event.

6.10 WELD STRESSES

Critical weld locations under seismic loading are at the bottom of the rack at the baseplate connection and at the welds on the support legs. Results from the dynamic analysis using the simulation codes are surveyed and the maximum loading is used to qualify the welds on these locations.

6.10.1 Baseplate to Rack Welds and Cell-to-Cell Welds

Section NF permits, for the SSE condition, an allowable weld stress $\tau = .42\ S_u = 28{,}600$ psi. Based on the worst case of all runs reported, the maximum weld stress for the baseplate to rack welds is 15860 psi for SSE conditions. This value occurs using a fuel weight of 1200 lbs. per cell. For normal fuel loading the weld stress under SSE at this location is reduced to 10785 psi.

The weld between baseplate and support leg is checked using limit analysis techniques. The structural weld at that location is considered safe if the interaction curve satisfies

$$F/F_y + M_b/M_y < 1$$

where F_y, M_y are the limit load and moment under direct load only and direct moment only. F, M_b are the absolute values of the actual peak force and moments applied to the weld section. This is a much more conservative relation than the actual interaction curve. For the worst case simulation, this criterion gives $F/F_y + M_b/M_y = .409$ for the support leg to baseplate weld.

The critical area that must be considered for fuel tube to fuel tube welds is the weld between the fuel tubes. This weld is discontinuous as we proceed along the tube length.

Stresses in the fuel tube to fuel tube welds develop along the length of each fuel tube due to fuel assembly impact with the tube wall. This occurs if fuel assemblies in adjacent tubes are moving out of phase with one another so that impact

loads in two adjacent tubes are in opposite directions which would tend to separate the channel from the tube at the weld. The critical load that can be transferred in this weld region for the SSE condition is calculated as 5056 lbs. at every fuel tube connection to adjacent tubes. An upper bound to the load required to be transferred is

$$\sqrt{2} \times 377.4 \times 2 = 1067 \text{ lbs.}$$

where we have used a maximum impact load of 377.4 lbs. (from Table 6.5), assumed two impact locations are supported by each weld region, and have increased the load by $\sqrt{2}$ to account for 3-D effects.

6.10.2 Heating of an Isolated Cell

Weld stresses due to heating of an isolated hot cell are also computed. The assumption used is that a single cell is heated, over its entire length, to a temperature above the value associated with all surrounding cells. No thermal gradient in the vertical direction is assumed so that the results are conservative. Using the temperatures associated with this unit, analysis shows that the weld stresses along the entire cell length do not exceed the allowable value for a thermal loading condition. Section 7 reports a value for this thermal stress.

6.11 SEISMIC QUALIFICATION USING MULTIPLE TIME HISTORIES

It is recognized that the time histories corresponding to a given spectrum are non-unique by definition. Therefore, to provide added confidence in the results, two additional sets of synthetic SSE time histories have been generated to investigate the sensitivity of rack behavior to different seismic events obtained from the same response spectrum. Figures 6.20 to 6.31

show the additional SSE's together with a comparison of the regenerated and the original spectrums. The events are designated as 2nd SSE (H4, H5, H6 time histories) and 3rd SSE (H7, H8, H9 time histories). Tables 6.7 and 6.8 are similar in content to Tables 6.5 and 6.6 and present the results of these additional analyses using the two new earthquake sets. While the individual results are different, as would be expected, the conclusions presented in Section 6.8 and 6.9 based on the base time history analysis remain the same.

6.12 MULTI-RACK ANALYSIS

Summary of Analysis

In order to further confirm the structural adequacy of the racks, a line of modules has been subjected to a single horizontal plus the vertical earthquakes to assess the implications of multi-rack effects. The model used and the methodology have been previously used in rack licensing efforts at other dockets, most recently Vogtle Unit 2, and have been approved by the USNRC. In order to examine maximum rack displacements, we assume that the 6x14 racks are turned 90 degrees to expose the direction kinematically more unstable to the seismic excitation direction.

Figure 6.32 shows the 2-D scenario studied for the five rack array. The following degrees-of-freedom are defined in the model shown here:

$x_1, x_5, x_9, x_{13}, x_{17}$	=	horizontal displacement of rattling fuel
$x_2, x_6, x_{10}, x_{14}, x_{18}$	=	horizontal displacement of mass center of rack

$\phi_3, \phi_7, \phi_{11}, \phi_{15}, \phi_{19}$	=	clockwise rotation of rack module
$x_4, x_8, x_{12}, x_{16}, x_{20}$	=	vertical displacement of rack plus fuel

The gap elements 3, 4, 10, 11, 16, 17, 22, 23, 28, 29 represent impact springs to track rattling fuel-to-fuel-cell impact loads as a function of time. Gap elements 1, 2, 5, 6, 9, 12, 15, 18, 21, 24, 27 and 30 are impact springs used to track potential rack-to-wall or rack-to-rack impacts. Gap elements 7, 8, 13, 14, 19, 20, 25, 26, 31, 32 are impact springs to track the vertical load in the support feet in each rack. Each spring represents the cumulative stiffness of two support feet reflecting the two dimensional nature of the model.

Finally, friction elements are used at each support location to simulate the potential for sliding. The limiting load in each friction element is based on the instantaneous load in the gap element associated with the support.

Fluid coupling associated with the fluid external to the racks is included in the model. The three dimensional nature of the external fluid coupling is accounted for by conservatively assuming a larger than actual hydrodynamic gap parallel to the horizontal direction of the earthquake when computing the contribution to hydrodynamic mass due to cross coupling of the motion. This conservatively limits the fluid coupling contribution of the flow in fluid gaps parallel to the horizontal excitation direction and is consistent with the USNRC position in this matter.

Fluid coupling between fuel and rattling mass is included. Based on the fuel configuration, we can estimate the kinetic energy of the fluid flow in a conservative manner and include the appropriate coupling effect in the analysis.

The kinetic energy and generalized forces of the structural assemblage shown in Figure 6.32 can be determined and the governing equations developed by applying the Lagrangian techniques. The USNRC qualified computer code DYNARACK used in the single rack 3-D analysis is then used to study the behavior of the assemblage under the postulated seismic loading for the plant.

Referring to Section 2 of this report, the particular modules studied are Modules A (next to the South Wall), B1, B2, C1, and C2 (next to the North Wall). This array is chosen because it contains the largest racks and, a rack with the largest length to width ratio. This array also has a low rack-to-wall coupling contribution, which would maximize the kinematic response of the racks. As noted earlier, we have turned the C racks in this model to expose the weakest direction to an overturning moment.

All of the cells in all of the racks are assumed fully occupied with normal fuel assemblies. This is the critical case based on the single rack analysis results.

The coefficient of friction, μ, is .5 and is kept constant through the entire event. This is the mean value of the

coefficient of friction expected in the pool. The earthquakes applied are the N-S SSE and the vertical SSE. A similar model has been employed in a previous licensing submittal for Vogtle Unit 2.

The support feet are modelled by gap elements and the bearing pad areas accounted for in the calculation of the pool floor stiffness.

Table 6.9 summarizes the design basis values used in the simulation run.

Table 6.10 summarizes the results of the regular fuel multi-rack analysis and demonstrates that there are no rack-to-rack impacts or rack-to-wall impacts. The results show that the support foot loads are consistent with the single rack simulations. Figures 6.33 to 6.35 show the time history of the gaps between modules B1 and B2, B2 and C1, and C1 and C2. Figure 6.36 shows that the support foot movement for rack B2 is quite small. This is typical for all racks in the analysis. The kinematic results obtained from the 2-D multi-rack have the same orders of magnitude as the 3-D single rack analyses.

6.13 DEFINITION OF TERMS USED IN SECTION 6.0

S1, S2, S3, S4	Support designations
p_i	Absolute degree-of-freedom number i
q_i	Relative degree-of-freedom number i
μ	Coefficient of friction

U_i	Pool floor slab displacement time history in the i-th direction
x,y coordinates	horizontal direction
z coordinate	vertical direction
K_I	Impact spring between fuel assemblies and cell
K_f	Linear component of friction spring
K_S	Axial spring at support leg locations
N	Compression load in a support foot
K_R	Rotational spring provided by the pool slab
Subscript i	When used with U or X indicates direction (i = 1 x-direction, i = 2 y-direction, i = 3 z-direction)

6.14 REFERENCES

6.1 USNRC Standard Review Plan, NUREG-0800 (1981).

6.2 ASME Boiler & Pressure Vessel Code, Section III, Subsection NF (1983).

6.3 USNRC Regulatory Guide 1.29, "Seismic Design Classification," Rev. 3, 1978.

6.4 "Friction Coefficients of Water Lubricated Stainless Steels for a Spent Fuel Rack Facility," Prof. Ernest Rabinowicz, MIT, a report for Boston Edison Company, 1976.

6.5 USNRC Regulatory Guide 1.92, "Combining Modal Responses and Spatial Components in Seismic Response Analysis," Rev. 1, February, 1976.

6.6 "The Component Element Method in Dynamics with Application to Earthquake and Vehicle Engineering," S. Levy and J.P.D. Wilkinson, McGraw Hill, 1976.

6.7 "Dynamics of Structures," R.W. Clough and J. Penzien, McGraw Hill (1975).

6.8 "Mechanical Design of Heat Exchangers and Pressure Vessel Components," Chapter 16, K.P. Singh and A.I. Soler, Arcturus Publishers, Inc., 1984.

6.9 R.J. Fritz, "The Effects of Liquids on the Dynamic Motions of Immersed Solids," Journal of Engineering for Industry, Trans. of the ASME, February 1972, pp 167-172.

6.10 "Dynamic Coupling in a Closely Spaced Two-Body System Vibrating in Liquid Medium: The Case of Fuel Racks," K.P. Singh and A.I. Soler, 3rd International Conference on Nuclear Power Safety, Keswick, England, May 1982.

6.11 USNRC Regulatory Guide 1.61, "Damping Values for Seismic Design of Nuclear Power Plants," 1973.

6.12 "OT Position for Review and Acceptance of Spent Fuel Storage and Handling Applications", dated April 14, 1978, and January 18, 1979 amendment thereto.

Table 6.1

DEGREES OF FREEDOM

Location (Node)	Displacement U_x	U_y	U_z	Rotation θ_x	θ_y	θ_z
1	P_1	P_2	P_3	q_4	q_5	q_6
2	P_{17}	P_{18}	P_{19}	q_{20}	q_{21}	q_{22}
	Point 2 is assumed attached to rigid rack at the top most point.					
2*	P_7	P_8				
3*	P_9	P_{10}				
4*	P_{11}	P_{12}				
5*	P_{13}	P_{14}				
1*	P_{15}	P_{16}				

where:

$P_i = q_i(t) + U_1(t)$ $\quad i = 1,7,9,11,13,15,17$

$= q_i(t) + U_2(t)$ $\quad i = 2,8,10,12,14,16,18$

$= q_i(t) + U_3(t)$ $\quad i = 3,19$

$U_i(t)$ are the 3 known earthquake displacements.

Table 6.2
NUMBERING SYSTEM FOR GAP ELEMENTS AND FRICTION ELEMENTS

I. Nonlinear Springs (Gap Elements) (64 Total)

Number	Node Location	Description
1	Support S1	Z compression only element
2	Support S2	Z compression only element
3	Support S3	Z compression only element
4	Support S4	Z compression only element
5	2,2*	X rack/fuel assembly impact element
6	2,2*	Y rack/fuel assembly impact element
7	2,2*	Y rack/fuel assembly impact element
8	2,2*	Y rack/fuel assembly impact element
9-24	Other rattling masses for nodes 1*, 3*, 4* and 5*	
25	Bottom cross-section of rack (around edge)	Inter-rack impact elements
.		Inter-rack impact elements
.		Inter-rack impact elements
.		Inter-rack impact elements
.		Inter-rack impact elements
.		Inter-rack impact elements
.		Inter-rack impact elements
44		Inter-rack impact elements
45	Top cross-section of rack (around edge)	Inter-rack impact elements
.		Inter-rack impact elements
.		Inter-rack impact elements
.		Inter-rack impact elements
.		Inter-rack impact elements
.		Inter-rack impact elements
.		Inter-rack impact elements
64		Inter-rack impact elements

Table 6.2 (continued)

NUMBERING SYSTEM FOR GAP ELEMENTS AND FRICTION ELEMENTS

II. Friction Elements (16 total)

Number	Node Location	Description
1	Support S1	X direction friction
2	Support S1	Y direction friction
3	Support S2	X direction friction
4	Support S2	Y direction friction
5	Support S3	X direction friction
6	Support S3	Y direction friction
7	Support S4	X direction friction
8	Support S4	Y direction friction
9	S1	X Slab moment
10	S1	Y Slab moment
11	S2	X Slab moment
12	S2	Y Slab moment
13	S3	X Slab moment
14	S3	Y Slab moment
15	S4	X Slab moment
16	S4	Y Slab moment

Table 6.3

TYPICAL INPUT DATA FOR RACK ANALYSES (lb-inch units)

		Module B	Module C
Support Foot Spring Constant K_s (#/in.)		4.37×10^6	4.41×10^6
Frictional Spring Constant K_f (#/in.)		1.061×10^8	1.061×10^8
Rack to Fuel Assembly Impact Spring Constant (#/in.)		$.409 \times 10^6$ (x) $.487 \times 10^6$ (y)	$.382 \times 10^6$ (x) 2.13×10^6 (y)
Elastic Shear Spring for Rack (#/in.)		56421. (x) 79507. (y)	8097 (x) 218963. (y)
Elastic Bending Spring for Rack (#-in/in.)		8.244×10^9 (y) 9.798×10^9 (x)	1.60×10^9 (y) 8.469×10^9 (y)
Elastic Extensional Spring (#/in.)		1.99×10^7	1.267×10^7
Elastic Torsional Spring (#-in./in.)		1.83×10^8	1.087×10^8
Foundation Rotational Resistance Springs K_R (#-in./in.)		4.586×10^7	4.586×10^7
Gaps (in.) (for hydrodynamic calculations)			
(h_1, h_3 are -,x faces; and h_2, h_4 are -,+ y faces, respectively)	h_1	1.25	2.5
	h_2	.75	.75
	h_3	2.5	10.
	h_4	.75	10.

Table 6.4

RACK MATERIAL DATA

Material	Young's Modulus E (psi)	Yield Strength S_y (psi)	Ultimate Strength S_u (psi)
304L S.S.	27.9×10^6	23150	68100
Section III Reference	Table I-6.0	Table I-2.2	Table I-3.2

SUPPORT MATERIAL DATA

	Material			
1	ASTM-240, Type 304L (upper part of support feet)	27.9×10^6 psi	23,150 psi	68,100 psi
2	ASTM 564-630	27.9×10^6 psi	101,040 psi	145,000 psi

TABLE 6.5
STRESS FACTORS AND RACK TO FUEL IMPACT LOAD

Run	Remarks	Rack/Fuel Impact Load (#) (Per Cell)	STRESS FACTORS R_1	R_2	R_3
C01	Rack C Full Load 6x14 Heavier Fuel Cof = .8, SSE	377.4	.022 ——— .224	.017 ——— .041	.133* ——— .175**
C02	Rack C SSE, COF = .8 Full Load, Regular Fuel	339.	.015 ——— .159	.011 ——— .027	.101 ——— .168
C03	Rack C COF = .8 Full Load Heavier Fuel 1.5 SSE in horizontal directions (stability check)	N/A	N/A (Not applicable for this case)	N/A	N/A
C04	Rack C SSE, COF = .8 8 Cells centrally Loaded, Regular Fuel	63.	.008 ——— .037	.003 ——— .007	.036 ——— .064
B14	Rack B1 Cof = .8 Full Load, OBE 11x12 Heavier Fuel	Negligible Impact load	.019 ——— .220	.006 ——— .012	.004 ——— .084

* Upper values are for rack baseplate section.

** Lower values are for support foot cross section (upper part) See continuation of table for stress factors R_4-R_7).

Table 6.5 (continued)

Run	Remarks	Rack/Fuel Impact Load (#) (Per Cell)	STRESS FACTORS R_1	R_2	R_3
B13	Rack B1 Cof = .8, SSE Full Load Heavier Fuel	245.	.026 .325	.012 .023	.109* .209**
B12	Rack B1 Cof = .2, SSE Full Load, Regular Fuel	124.	.016 .172	.008 .019	.050 .206
B11	Rack B1 Full load, Regular Fuel Cof = .8, OBE	Negligible Impact Load	.014 .303	.004 .162	.003 .397
B10	Rack B1 Cof = .8 Full Load, SSE .6 Regular Fuel	124.	.016 .172	.008 .019	.050 .206

* Upper values are for rack baseplate section.

** Lower values are for support foot cross section (upper part) See continuation of table for stress factors R_4-R_7).

Table 6.5 (continued)

Run	Remarks	Rack/Fuel Impact (Per Cell)	STRESS FACTORS R_4	R_5	R_6	R_7
C01	See previous pages for these columns		.139	.196	.229	.018
			.254	.407	.443	.025
C02			.074	.144	.169	.015
			.169	.262	.293	.026
C03			N/A	N/A	N/A	N/A
C04			.01	.042	.048	.004
			.051	.089	.099	.01
B14			.004	.020	.021	.006
			.088	.271	.282	.012
B13			.082	.151	.177	.017
			.159	.508	.539	.032
B12			.035	.072	.084	.012
			.129	.334	.365	.030

Table 6.5
(continued)

Run	Remarks	Rack/Fuel Impact (Per Cell)	STRESS FACTORS R_4	R_5	R_6	R_7
B11	See previous pages for these columns		.003	.016	.017	.004
			.061	.162	.170	.008
B10			.034	.072	.084	.012
			.103	.298	.322	.024

Table 6.6
RACK DISPLACEMENTS AND SUPPORT LOADS
(all loads are in lbs.)

RUN****	FLOOR LOAD (sum of all support feet)	MAXIMUM SUPPORT LOAD	VERTICAL LOAD*	SHEAR LOAD**	DX (in.)	DY (in.)
C01	1.27×10^5	1 44990.	52080	4147	.6682	.0811***
		2 43700.	30502	6787	.0026	.0008
		3 48940.				
		4 52080.				
C02	7.16×10^4	1 2.75×10^4	34610.	1018.	.3826	.0626
		2 2.840×10^4	11693.	4313.	.0017	.0007
		3 3.265×10^4				
		4 3.461×10^4				
C03	N/A	N/A	N/A	N/A	1.039	.1071
					.0043	.0011
C04	1.621×10^4	1 8.253×10^3	8253.	977.	.0588	.0258
		2 7.896×10^3	7393.	1454.	.0032	.0009
		3 6.834×10^3				
		4 7.073×10^3				

* The first line in any set of data is the maximum vertical load and the second line reported is the vertical load when the net horizontal shear at the liner is maximum.

** The first line is the net horizontal liner shear when the vertical load is maximum; the second line is the maximum value of the net horizontal shear on any single support foot.

*** The first line reports results at the top of the rack; the second line reports results at the baseplate; the times at which these maximums occur may be different.

**** See Table 6.5 for definition of runs.

Table 6.6 (Continued)

RACK DISPLACEMENTS AND SUPPORT LOADS
(all loads are in lbs.)

RUN	FLOOR LOAD (sum of all support feet)	MAXIMUM SUPPORT LOAD	VERTICAL LOAD*	SHEAR LOAD**	DX (in.)	DY (in.)
B14	1.924×10^5	1 48130.	48140.	65.	.008	.0072
		2 48080.	40441	1803.	.0000	.0000
		3 48090.				
		4 48140.				
B13	2.046×10^5	1 59820.	71120.	4871.	.1943	.2059
		2 71120.	34639	4873.	.0011	.0014
		3 61640.				
		4 70000.				
B12	1.150×10^5	1 36820.	37470.	2404.	.0798	.0939
		2 34240.	33715.	4459.	.0005	.0006
		3 37470.				
		4 32410.				
B11	1.131×10^5	1 28300.	28300.	46.	.0058	.005
		2 28260.	23053.	1255.	.0000	.0000
		3 28270.				
		4 28300.				
B10	1.150×10^5	1 36820.	37470.	2223.	.0797	.0936
		2 34190.	20548.	3599.	.0005	.0006
		3 37470.				
		4 32300.				

TABLE 6.7
STRESS FACTORS AND RACK TO FUEL IMPACT LOAD

Run	Remarks	Rack/Fuel Impact Load (#/Cell)	STRESS FACTORS R_1	R2	R3
b20	11x12, Full Normal	141	.015	.009	.036
	2nd SSE Cof. = .8		.174	.018	.115
C21	6x14, Full Heavier Fuel	373	.021	.012	.147
	2nd SSE Cof. = .8		.199	.018	.199
C22	6x14, Full Normal	304	.014	.009	.111
	2nd SSE Cof. = .8		.146	.022	[illegible]
C34	6x14, 8 Cells with fuel (normal)	55.	.008	.003	.032
	3rd SSE Cof. = .8		.045	.007	.079
C32	6x14, Full Normal	226.	.014	.009	.127
	3rd SSE Cof. = .8		.147	.022	.207
C31	6x14 Full Heavier Fuel Cof. = .8	381.	.021	.015	.151
			.236	.028	.280
C24	6x14, 8 Cells with normal fuel	85.	.009	.003	.033
	2nd SSE Cof. = .8		.037	.006	.070

Table 6.7 (continued)

Run	Remarks	Rack/Fuel Impact Load (#/Cell)	STRESS FACTORS R_1	R2	R3
b32	11x12, Full Normal fuel	159.	.015	.012	.066
	3rd SSE Cof. = .2		.204	.038	.252
b30	11x12, Full Normal fuel	159.	.015	.012	.066
	3rd SSE Cof. = .8		.205	.028	.387
b23	11x12, Full Heavier fuel	239.	.022	.015	.072
	2nd SSE Cof. = .8		.309	.030	.199
b22	11x12, Full Normal fuel	141.	.015	.010	.036
	2nd SSE Cof. = .2		.174	.022	.115

Table 6.7 (continued)

Run	Remarks	Rack/Fuel Impact (Per Cell)	STRESS FACTORS R_4	R5	R6	R7
b20	See previous pages for these columns		.060	.071	.082	.009
			.120	.254	.272	.017
C21			.071	.138	.161	.023
			.118	.364	.394	.030
C22			.062	.134	.156	.013
			.139	.259	.283	.024
C34			.018	.046	.053	.004
			.043	.118	.131	.012
C32			.077	.139	.162	.015
			.139	.290	.317	.032
C31			.120	.199	.233	.027
			.193	.406	.447	.040
C24			.008	.040	.046	.004
			.043	.096	.106	.043

Table 6.7 (continued)

Run	Remarks	Rack/Fuel Impact (Per Cell)	R4	R5	R6	R7
b32	See previous pages for these columns		.077	.114	.133	.011
			.257	.444	.490	.037
b30			.073	.111	.130	.012
			.139	.356	.387	.025
b23			.097	.118	.137	.015
			.202	.443	.468	.029
b22			.060	.071	.082	.009
			.151	.276	.298	.017

Table 6.8

RACK DISPLACEMENTS AND SUPPORT LOADS
For Additional Seismic Loads
(all loads are in lbs.)

RUN	FLOOR LOAD (sum of all support feet) ($\times 10^5$)	MAXIMUM SUPPORT LOAD ($\times 10^4$)		VERTICAL LOAD*	SHEAR LOAD**	DX (in.)	DY (in.)
b20	1.123	1	3.269	38120.	1418.	.1192	.0652
		2	3.754	20304.	2640.	.0008	.0005
		3	3.333				
		4	3.812				
c21	1.253	1	4.159	44210.	1551.	.3466	.0894
		2	4.103	16797.	4343.	.0013	.0009
		3	4.421				
		4	4.250				
c22	.71	1	3.032	31790.	1476.	.2857	.0671
		2	3.028	24354.	4012.	.0011	.0007
		3	3.179				
		4	3.072				
c34	.1495	1	.9796	9796.	1954.	.0904	.0254
		2	.9121	9796.	1954.	.0071	.0044
		3	.6759				
		4	.7205				
c32	.7056	1	3.162	32280	2439.	.3859	.0770
		2	3.079	20463	4621.	.0014	.0008
		3	3.228				
		4	3.197				

Table 6.8 (continued)

RACK DISPLACEMENTS AND SUPPORT LOADS
For Additional Seismic Loads
(all loads are in lbs.)

RUN	FLOOR LOAD (sum of all support feet) ($\times 10^5$)	MAXIMUM SUPPORT LOAD ($\times 10^4$)	VERTICAL LOAD*	SHEAR LOAD**	DX (in.)	DY (in.)
C31	1.243	1 4.823	51670.	3484.	.5984	.0918
		2 4.881	36229.	5857.	.0023	.0010
		3 5.080				
		4 5.167				
C24	.1773	1 .741	7993.	1598.	.0617	.0340
		2 .7467	7993.	1598.	.0347	.0108
		3 .7993				
		4. .7574				
b32	1.116	1 4.462	44620.	4497.	.181	.1215
		2 4.353	39074.	6658.	.0011	.0008
		3 4.415				
		4 4.473				
b30	1.116	1 4.455	44730.	.2269	.1732	.1215
		2 4.353	38396.	.4554	.0010	.0008
		3 4.380				
		4 4.473				
b23	1.986	1 6.112	67470.	2547.	.2287	.1309
		2 6.590	49234.	4333.	.0013	.0009
		3 5.869				
		4 6.747				
b22	1.123	1 3.27	38120.	1418.	.1192	.0652
		2 3.754	32084.	3234.	.0008	.0005
		3 3.340				
		4 3.812				

Table 6.9

Spring Constant Values for Multi-Rack Analysis

Rack-to-Fuel Gap Elements	$.409 \times 10^6$#/in	(A,B racks)
Support Foot Gap Elements	$.882 \times 10^7$#/in.	
Friction Elements	$.212 \times 10^{10}$	
Coefficient of Friction	.5	
Rack-to-Wall Impact Springs	$.1 \times 10^6$ (top of rack) $.2 \times 10^6$ (baseplate to wall)	
Rack-to-Rack Impact Springs	$.05 \times 10^6$ (top) $.1 \times 10^6$ (baseplate)	
Rack Height	171."	
Support Foot Height	11.625"	

	A	B-1	B-2	C-1	C-2
Width of each rack (in.)	70.25	70.25	70.25	89.375	89.375
Length of Rack (in.) (parallel to horizontal direction)	70.25	76.625	76.625	38.5	38.5
Rack Weight (lbs)	12800	13900	13900	8850	8850
Fuel Assembly Weight	643 lbs. per cell				
Side Gaps for Fluid Cross Coupling	7.5"				

Table 6.10

Results of Multi-Rack Analysis

Maximum Values	
Rack-to-Rack Impact Force	——— No Impacts ———
Rack-to-Wall Impact Force	——— No Impacts ———
Support Foot Loads	
Rack A	51950. lbs.
Rack B1	58450. lbs.
Rack B2	57400. lbs.
Rack C1	34200. lbs.
Rack C2	34245. lbs.
Upper Bound on Displacement at Top of Rack	
Rack A	.0733"
Rack B1	.08129"
Rack B2	.08149"
Rack C1	.07032"
Rack C2	.06524"
Cell-to-Fuel Assembly Impact Load Per Cell	
Rack A	82.4 lbs.
Rack B1	94.7 lbs.
Rack B2	113.3 lbs.
Rack C1	82.2 lbs.
Rack C2	74.9 lbs.

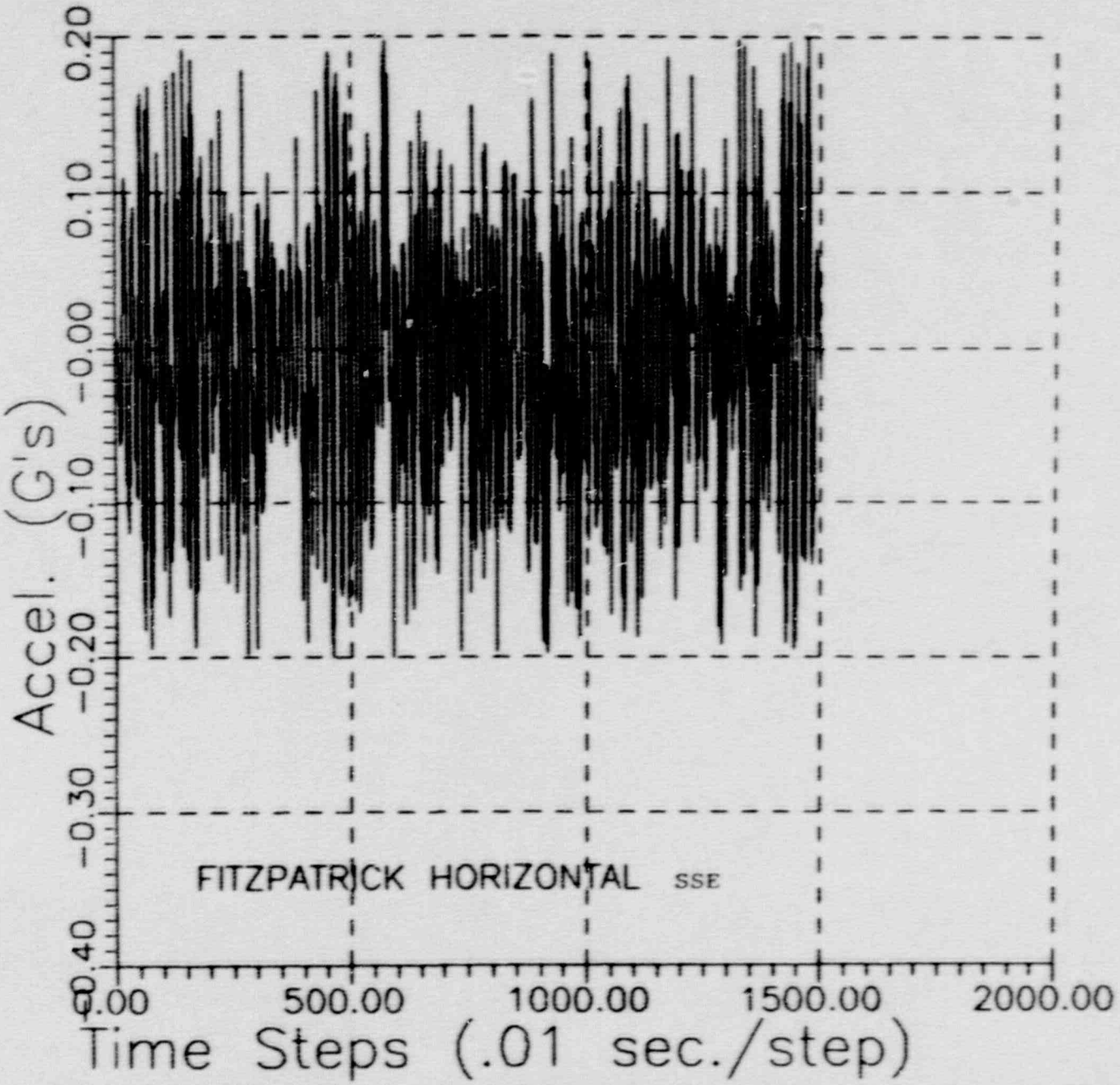
Accel. (G's)
0.20
0.10
-0.00
-0.10
-0.20
-0.30
-0.40
FITZPATRICK HORIZONTAL SSE
0.00
500.00
1000.00
1500.00
2000.00
Time Steps (.01 sec./step)

FIGURE 6.1

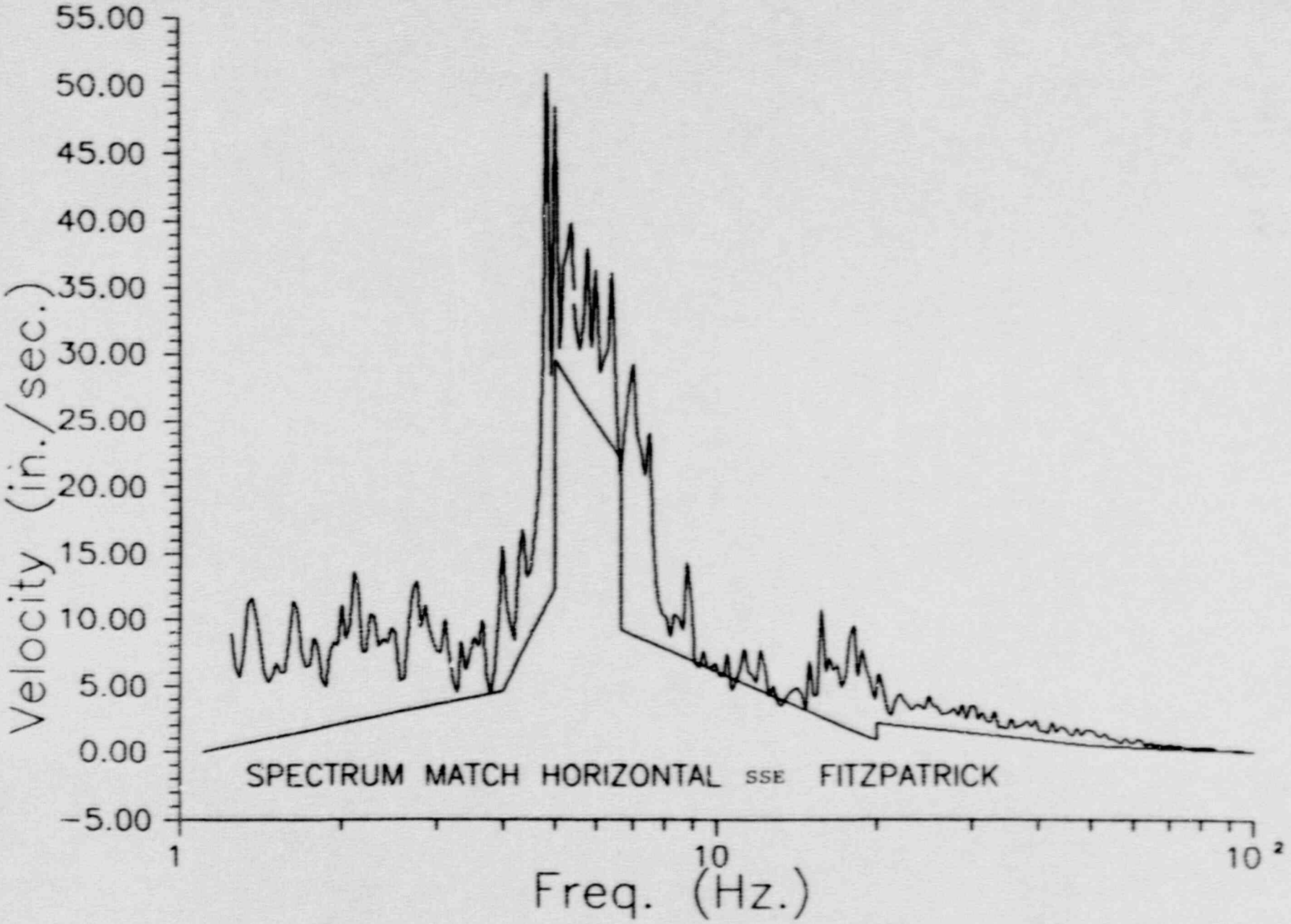

75-9

FIGURE 6.2

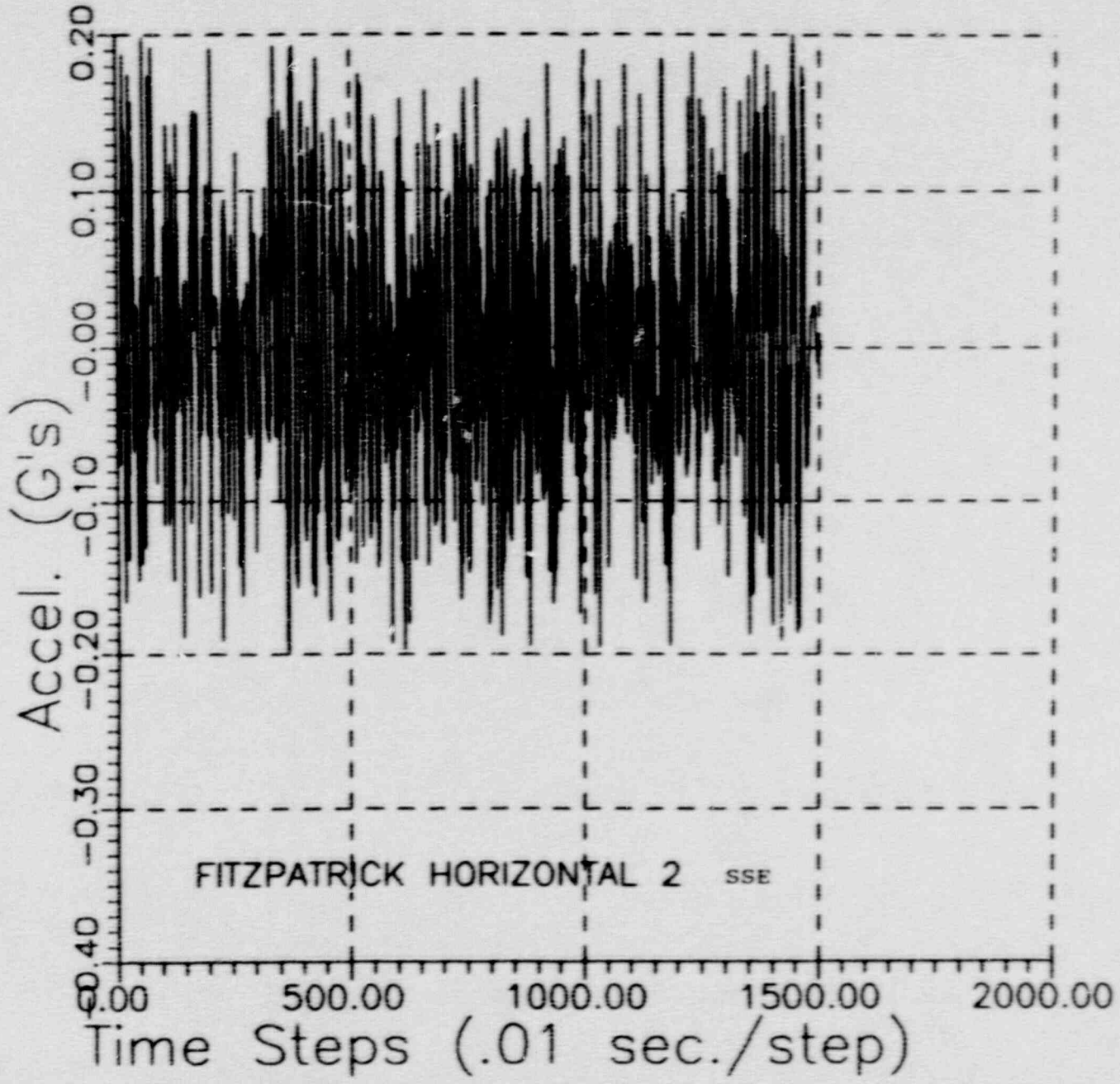
0.20
0.10
-0.00
-0.10
-0.20
-0.30
-0.40
Accel. (G's)
FITZPATRICK HORIZONTAL 2 SSE
0.00
500.00
1000.00
1500.00
2000.00
Time Steps (.01 sec./step)

FIGURE 6.3

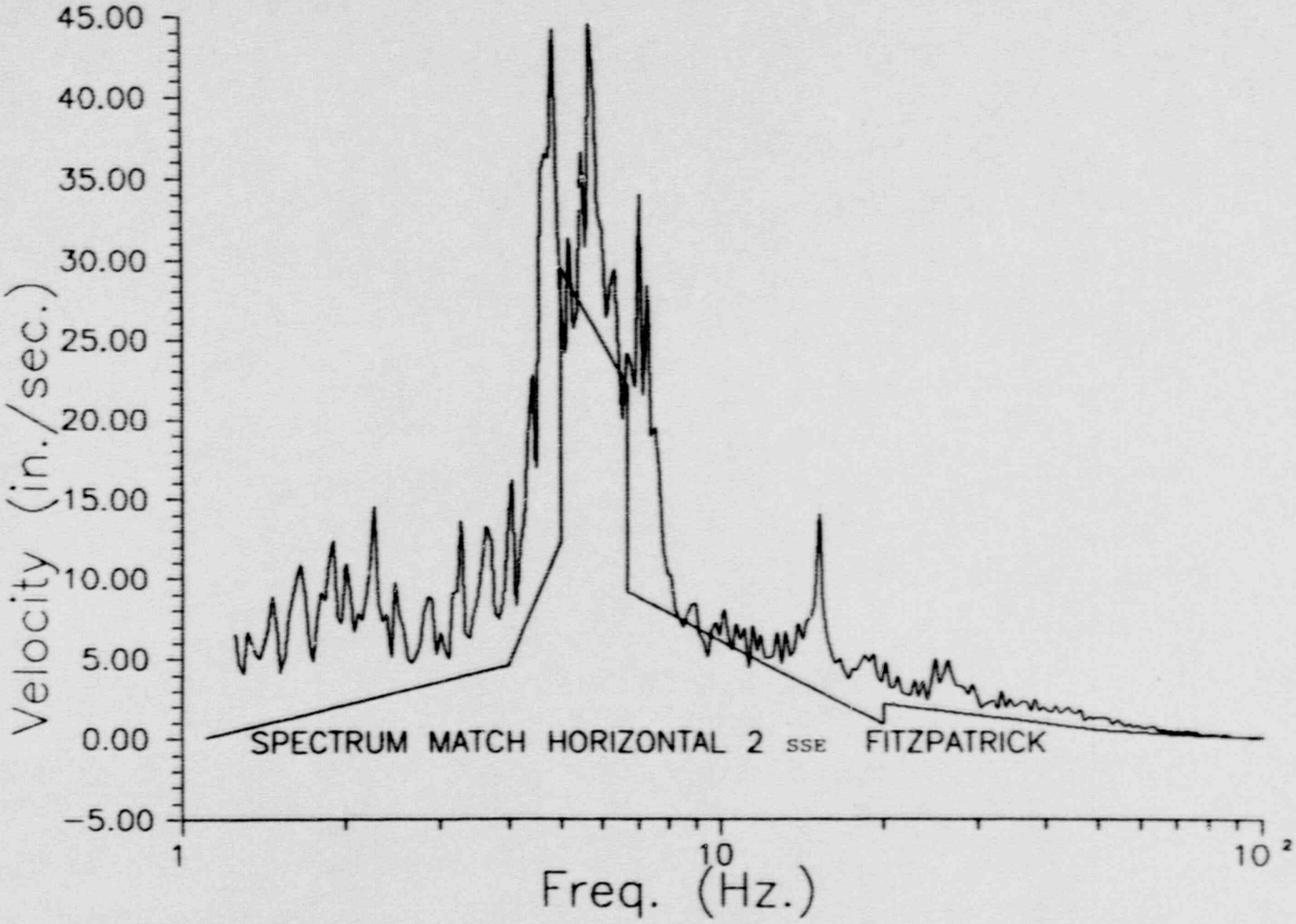
45.00
40.00
35.00
30.00
25.00
20.00
15.00
10.00
5.00
0.00
-5.00
Velocity (in./sec.)
SPECTRUM MATCH HORIZONTAL 2 SSE FITZPATRICK
1
10
10 2
Freq. (Hz.)

FIGURE 6.4

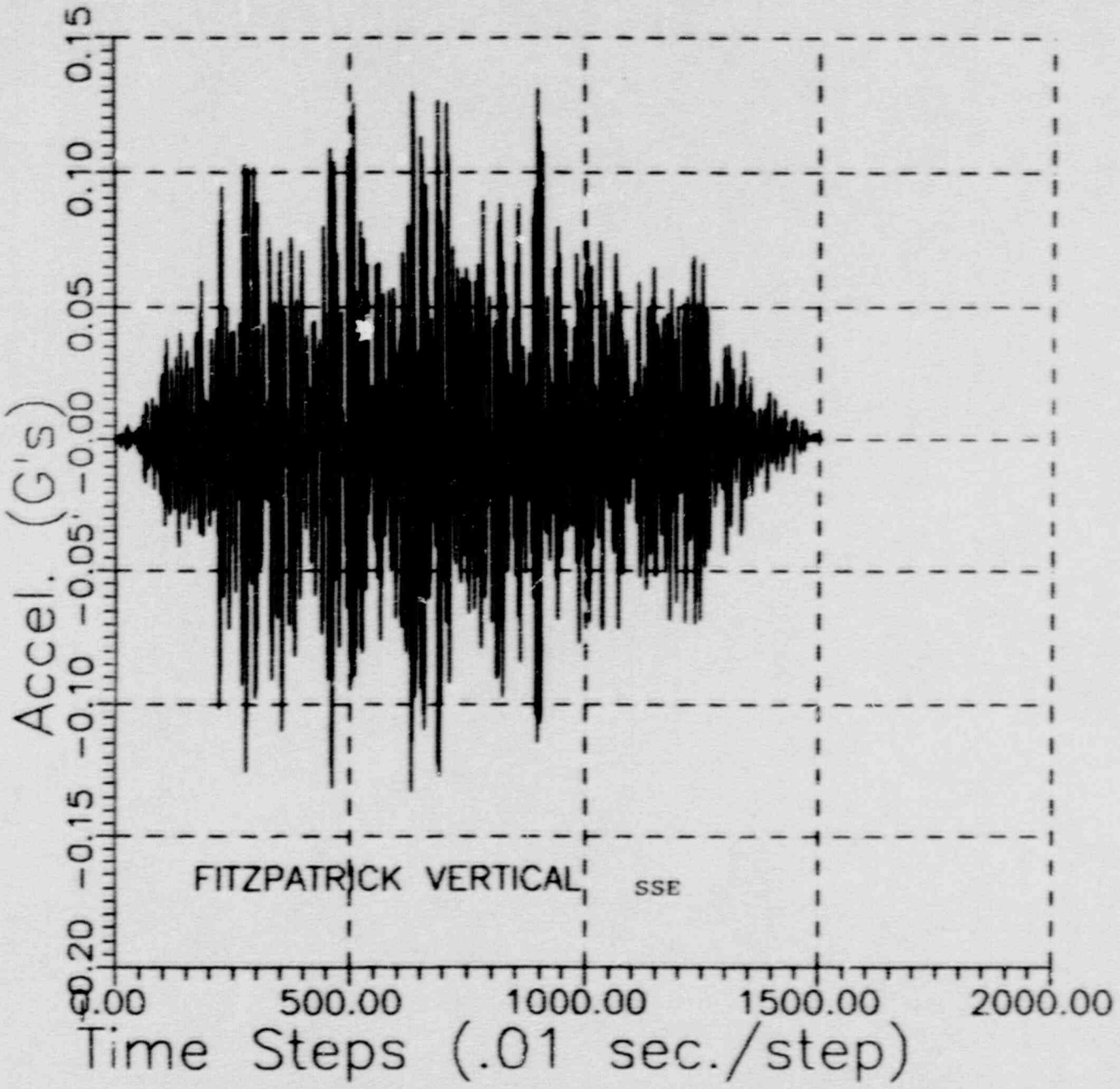
Accel. (G's)
0.15
0.10
0.05
-0.00
-0.05
-0.10
-0.15
-0.20
FITZPATRICK VERTICAL SSE
0.00
500.00
1000.00
1500.00
2000.00
Time Steps (.01 sec./step)

FIGURE 6.5

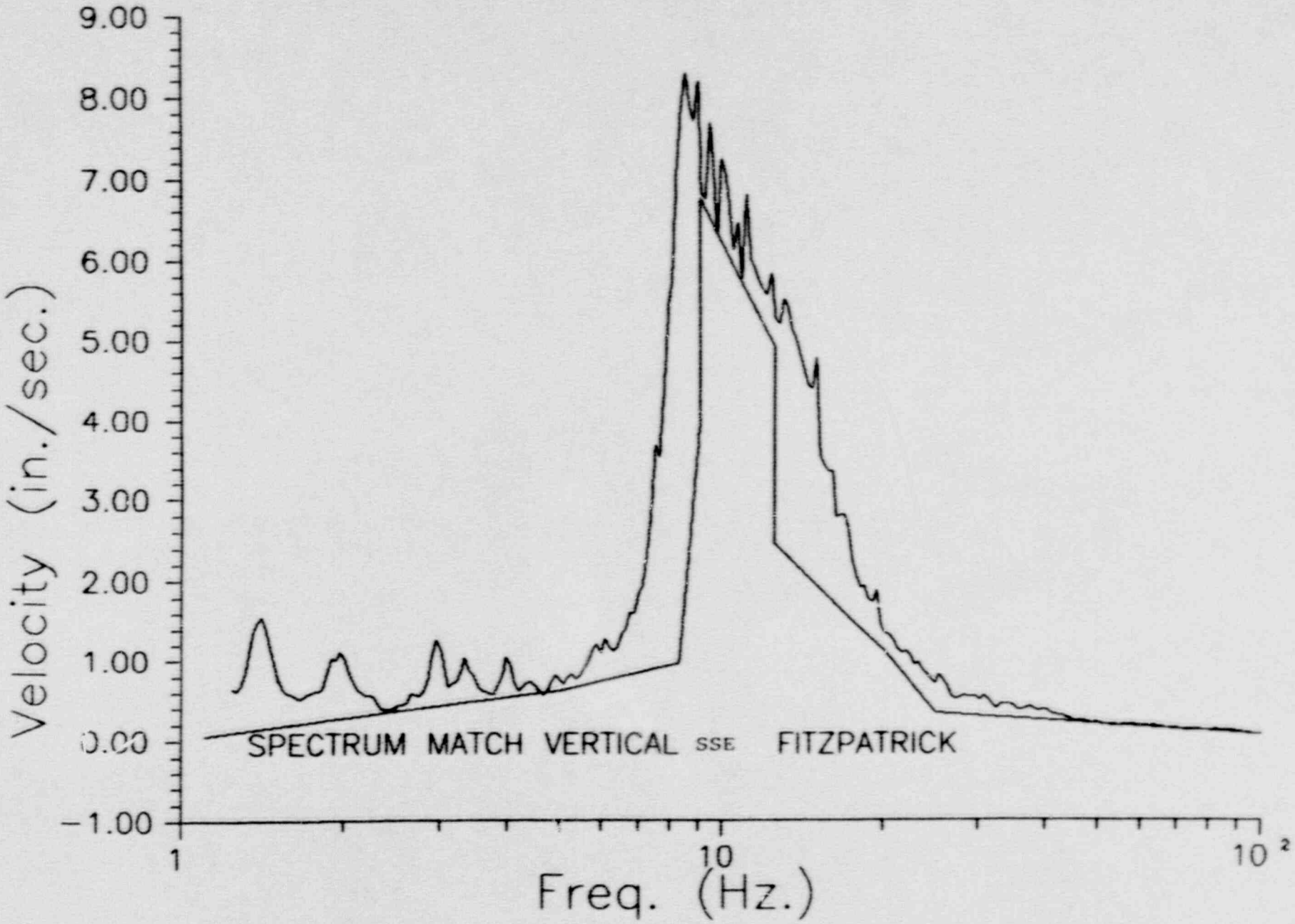
9.00
8.00
7.00
6.00
5.00
4.00
3.00
2.00
1.00
0.00
-1.00
Velocity (in./sec.)
SPECTRUM MATCH VERTICAL SSE FITZPATRICK
1
10
10 ²
Freq. (Hz.)

FIGURE 6.6

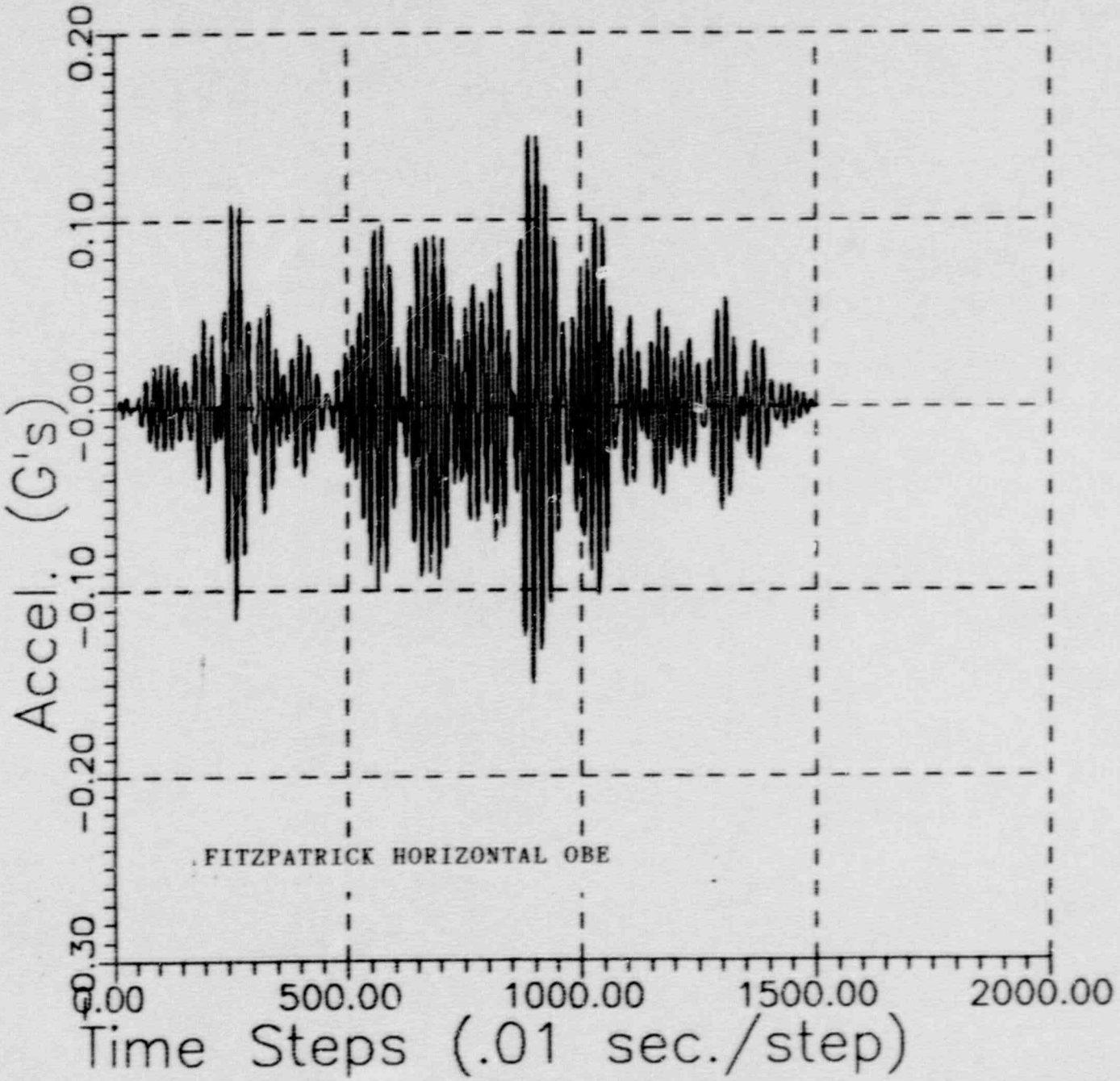
0.20
0.10
-0.00
-0.10
-0.20
-0.30
Accel. (G's)
FITZPATRICK HORIZONTAL OBE
0.00
500.00
1000.00
1500.00
2000.00
Time Steps (.01 sec./step)

FIGURE 6.7

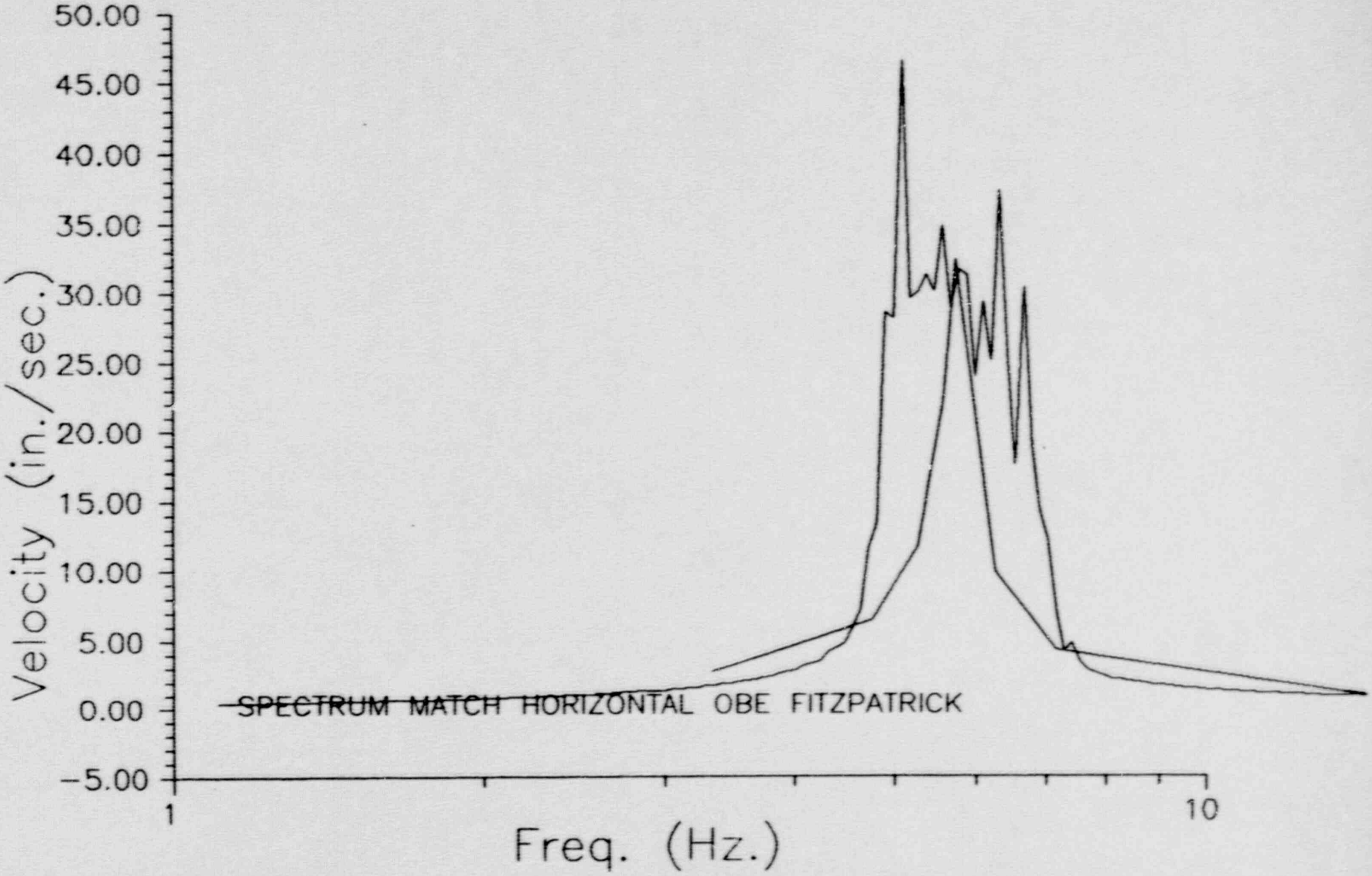
50.00
45.00
40.00
35.00
30.00
25.00
20.00
15.00
10.00
5.00
0.00
-5.00
Velocity (in./sec.)
1
10
Freq. (Hz.)
SPECTRUM MATCH HORIZONTAL OBE FITZPATRICK

FIGURE 6.8

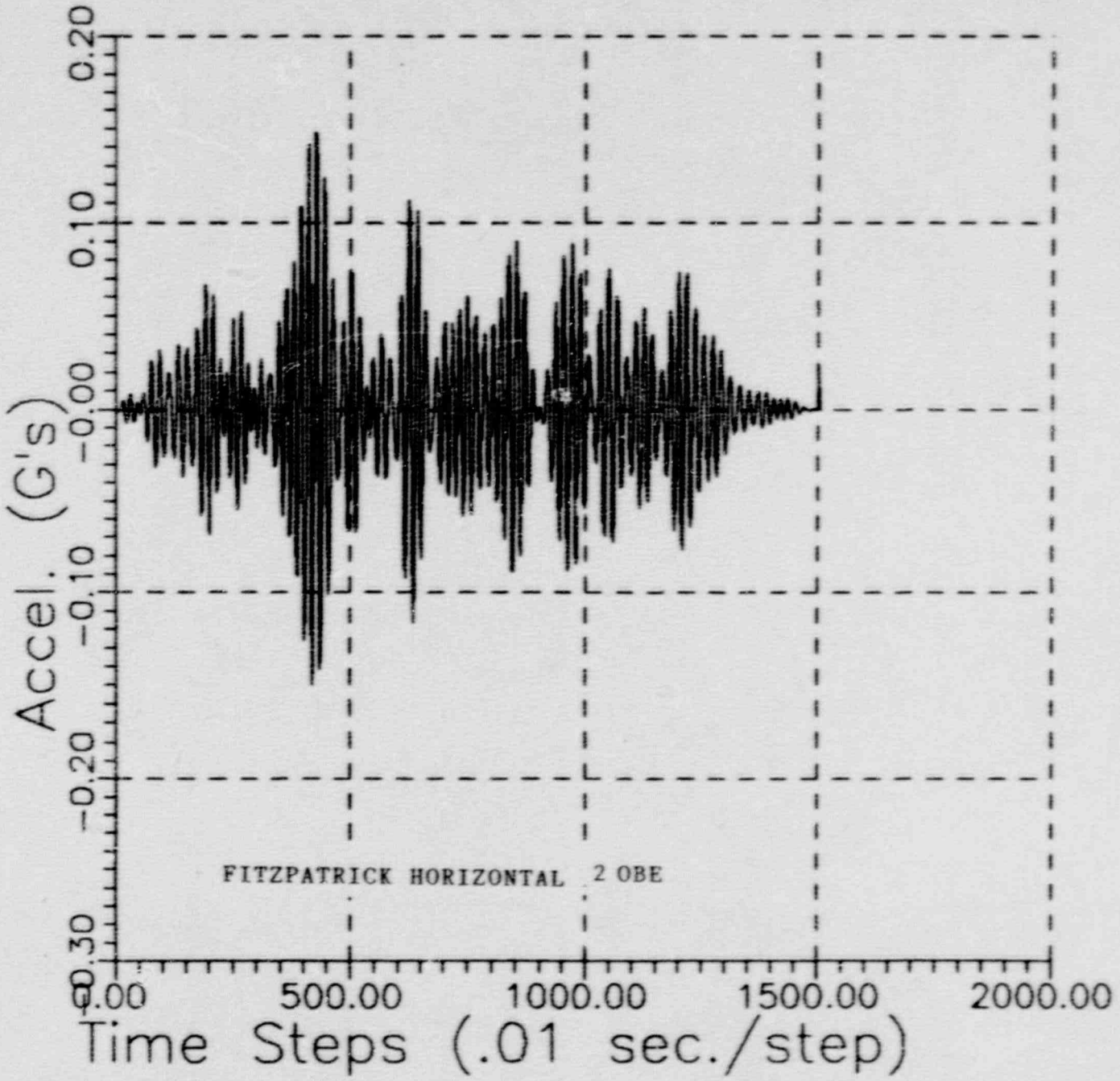
Accel. (G's)
0.20
0.10
-0.00
-0.10
-0.20
-0.30
0.00
500.00
1000.00
1500.00
2000.00
Time Steps (.01 sec./step)
FITZPATRICK HORIZONTAL 2 OBE

FIGURE 6.9

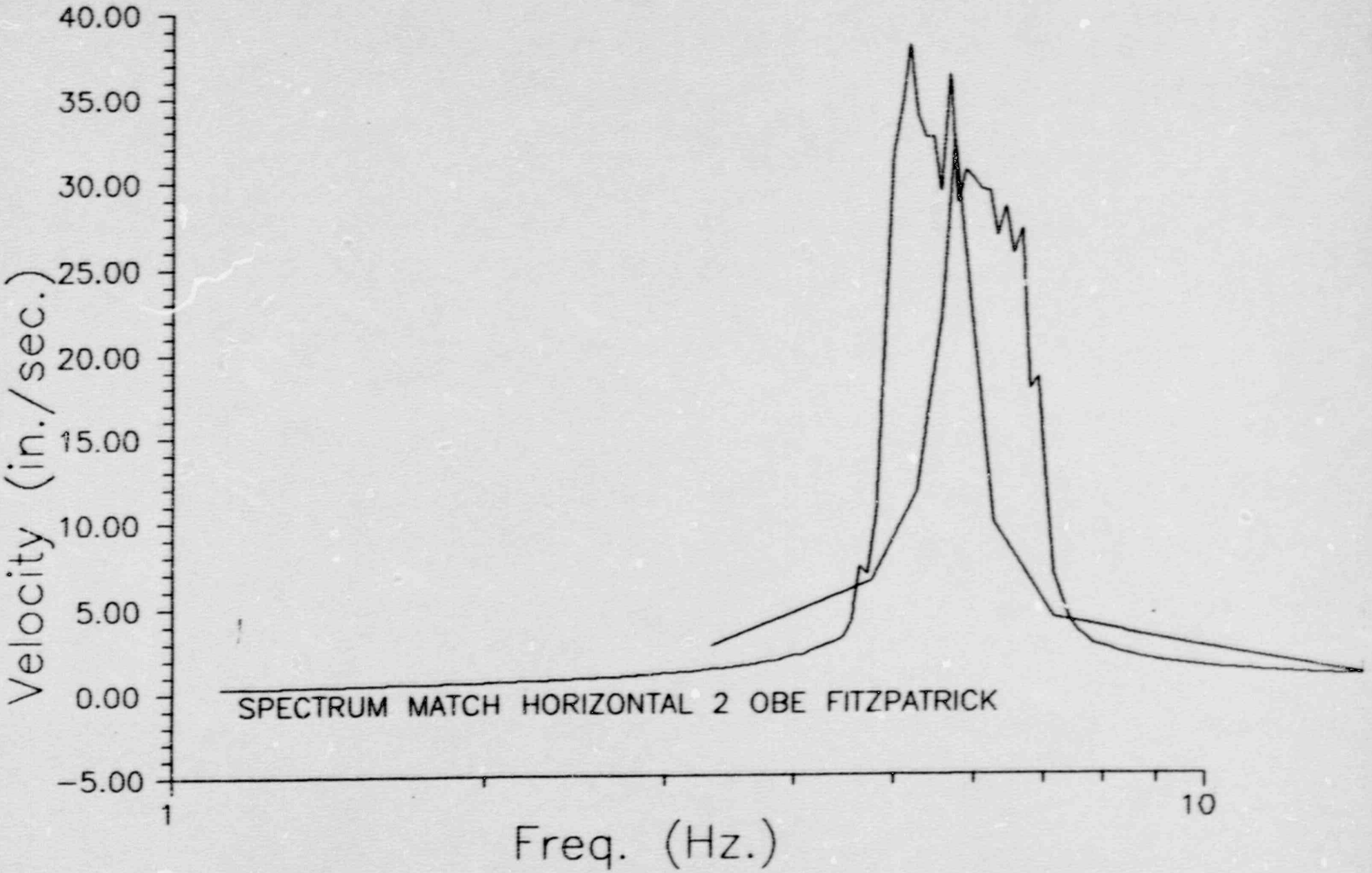
40.00
35.00
30.00
25.00
20.00
15.00
10.00
5.00
0.00
-5.00
Velocity (in./sec.)
SPECTRUM MATCH HORIZONTAL 2 OBE FITZPATRICK
1
10
Freq. (Hz.)

FIGURE 6.10

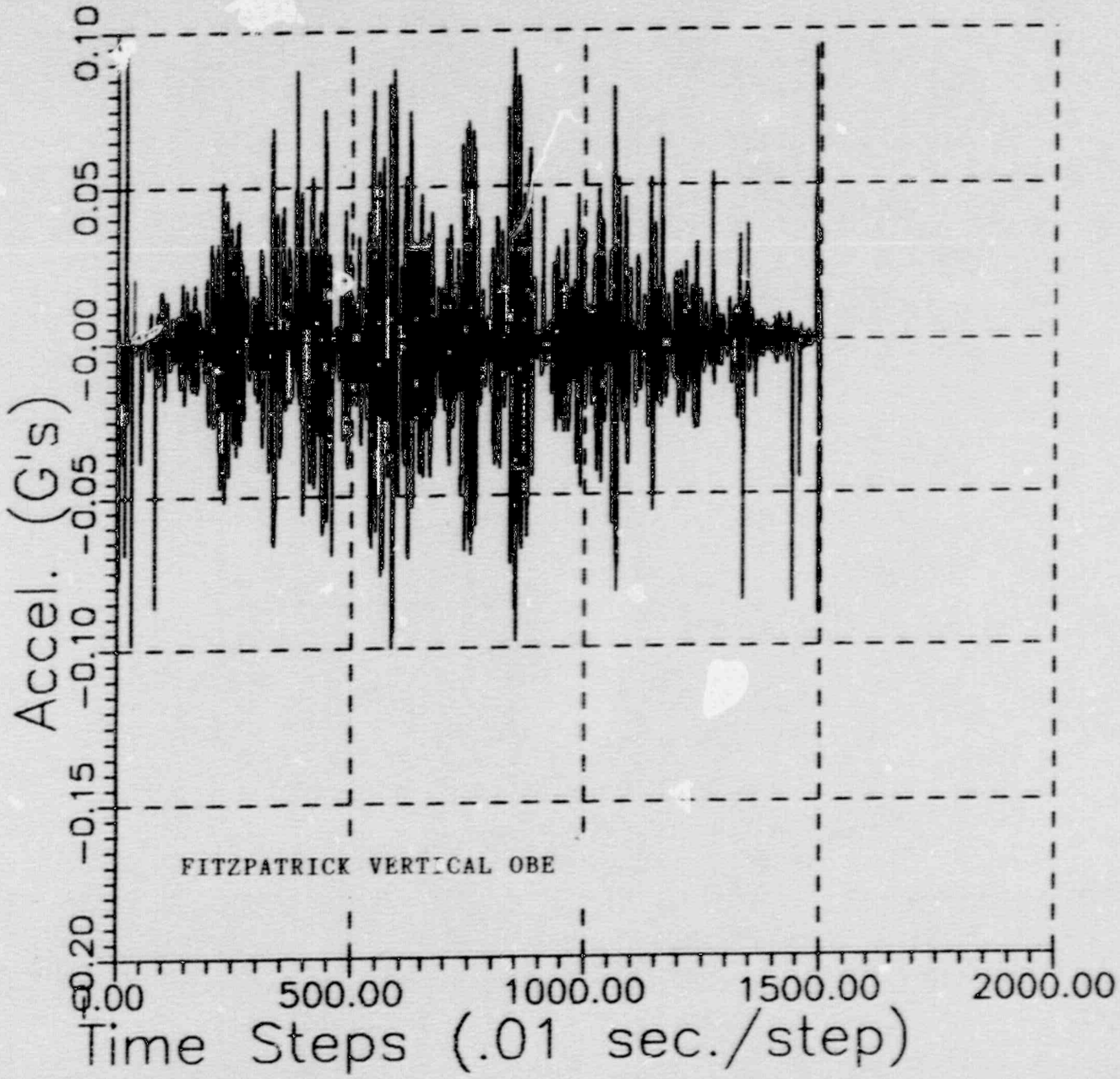
Accel. (G's)
0.10
0.05
-0.00
-0.05
-0.10
-0.15
-0.20
0.00
500.00
1000.00
1500.00
2000.00
Time Steps (.01 sec./step)
FITZPATRICK VERTICAL OBE

FIGURE 6.11

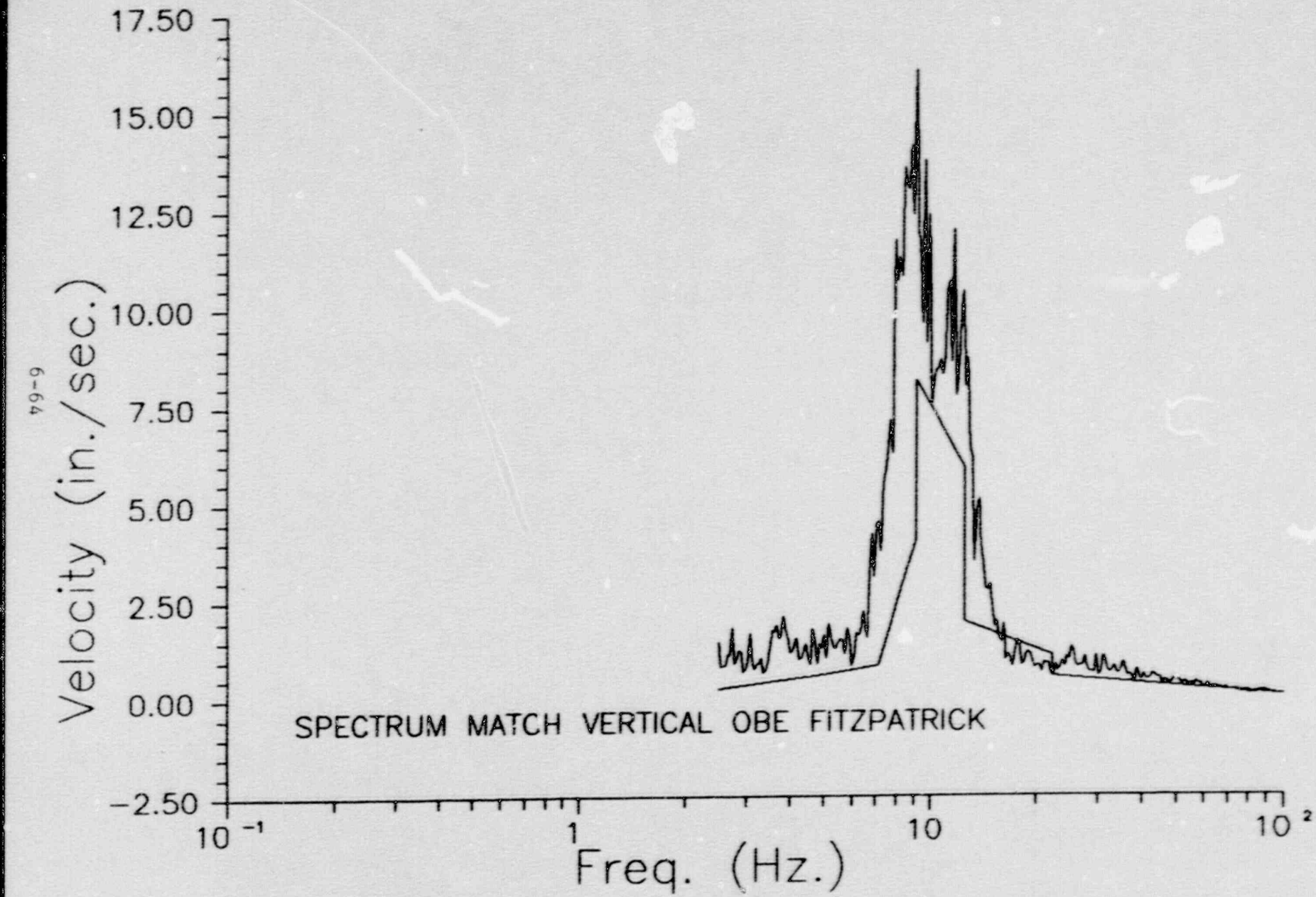
17.50
15.00
12.50
10.00
7.50
5.00
2.50
0.00
-2.50
Velocity (in./sec.)
SPECTRUM MATCH VERTICAL OBE FITZPATRICK
10 -1
1
10
10 2
Freq. (Hz.)

FIGURE 6.12

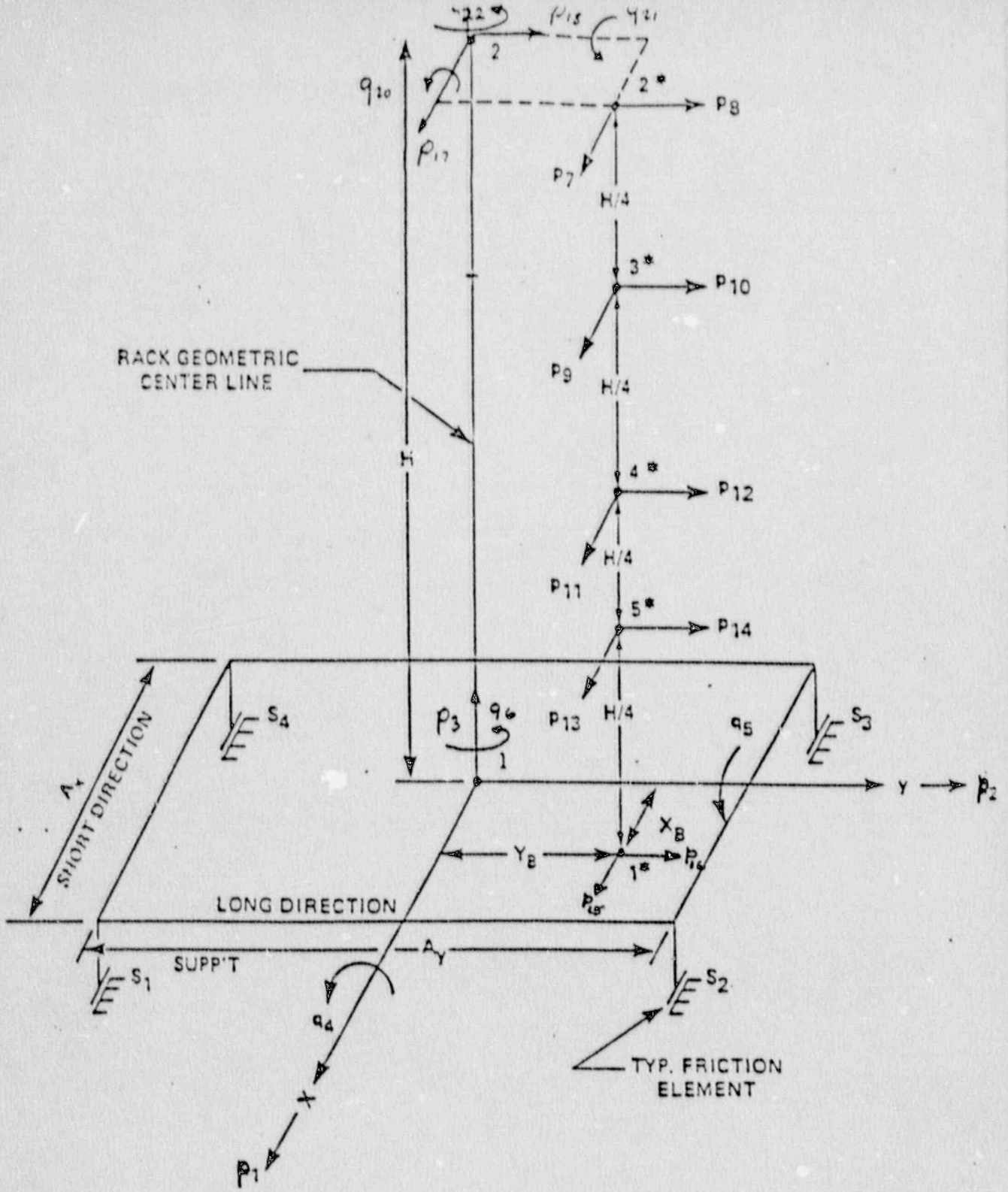

SCHEMATIC MODEL FOR DYNRACK

FIGURE 6.13

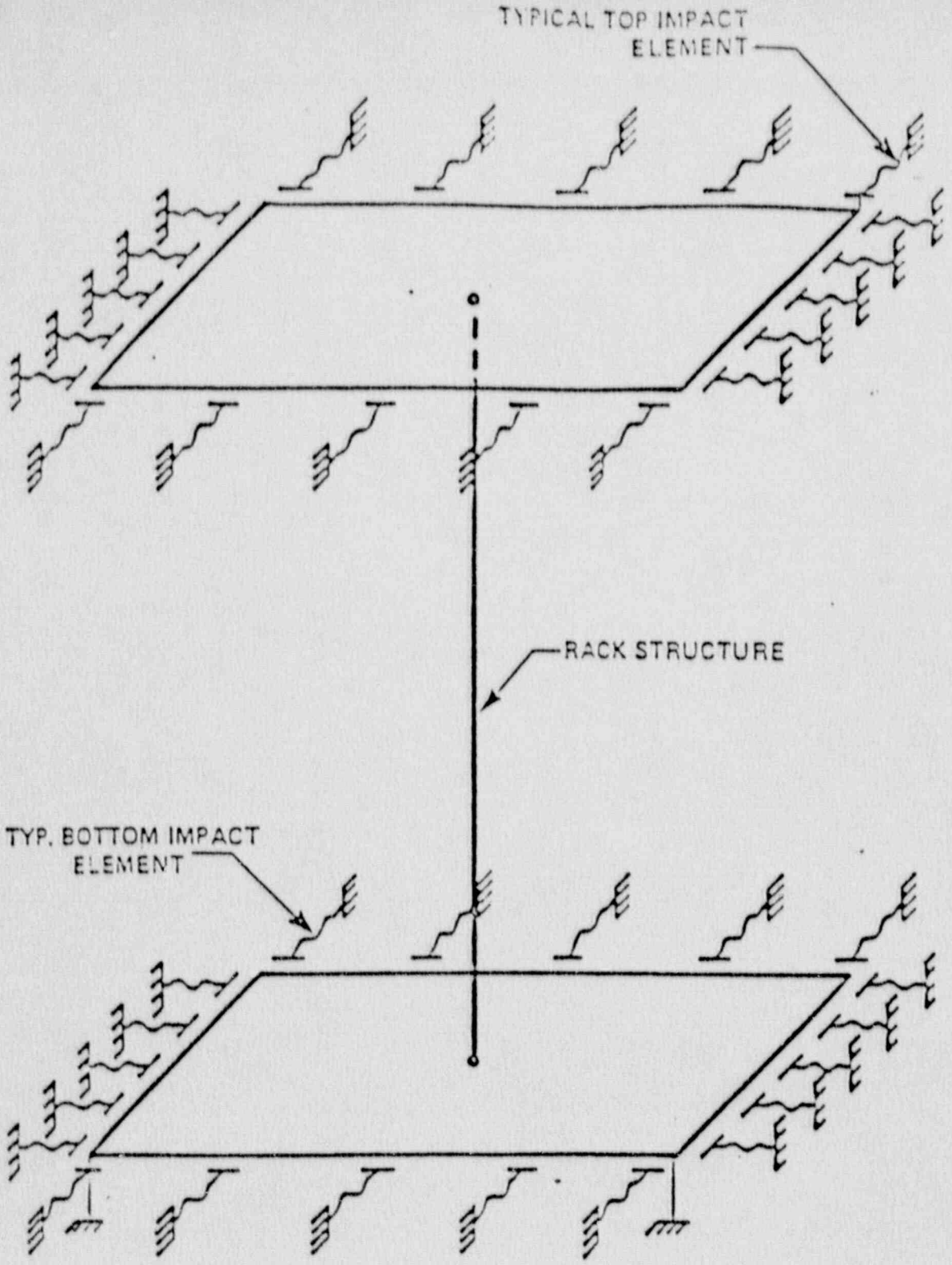

RACK-TO-RACK IMPACT SPRINGS

FIGURE 6.14

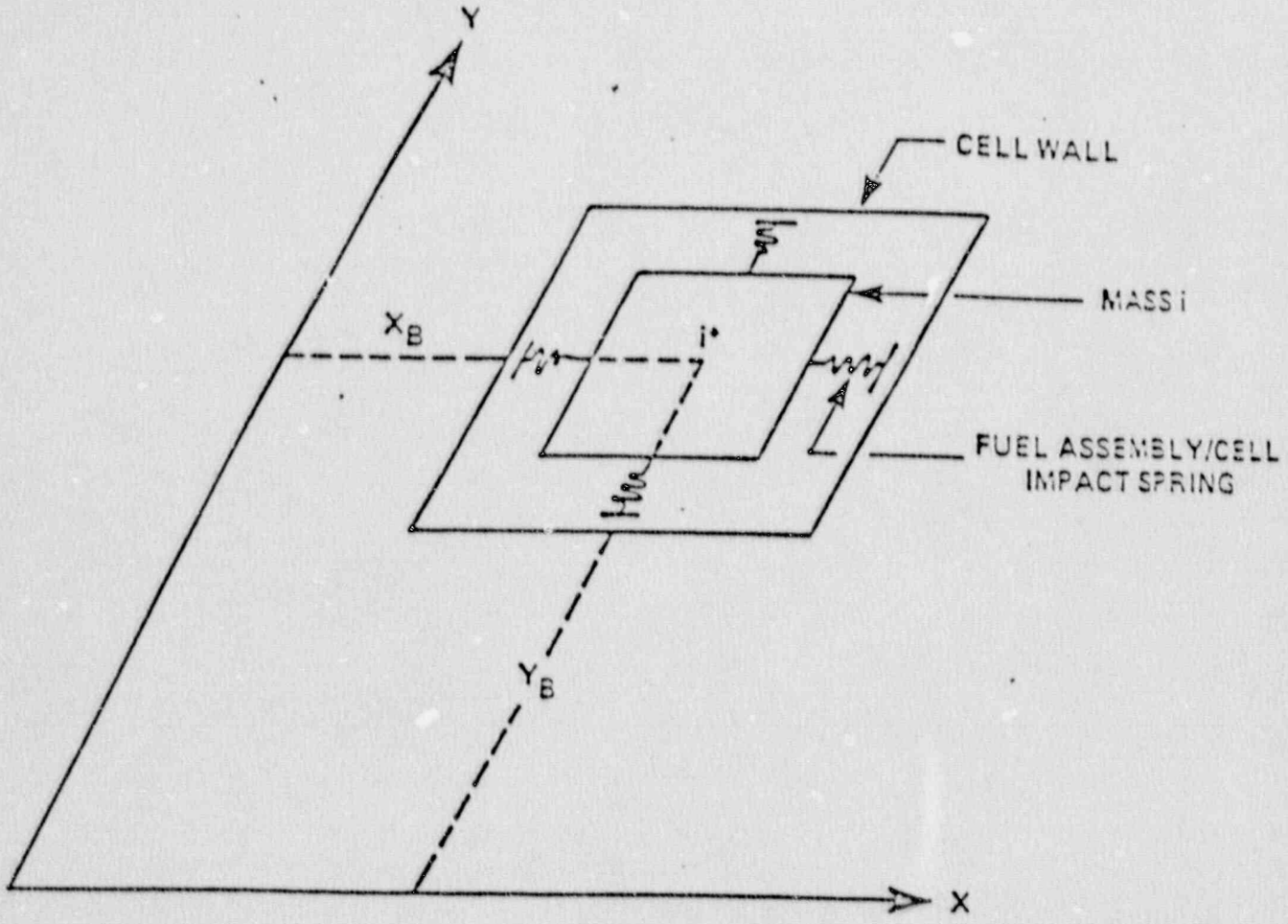

IMPACT SPRING ARRANGEMENT
AT NODE i

FIGURE 6.15

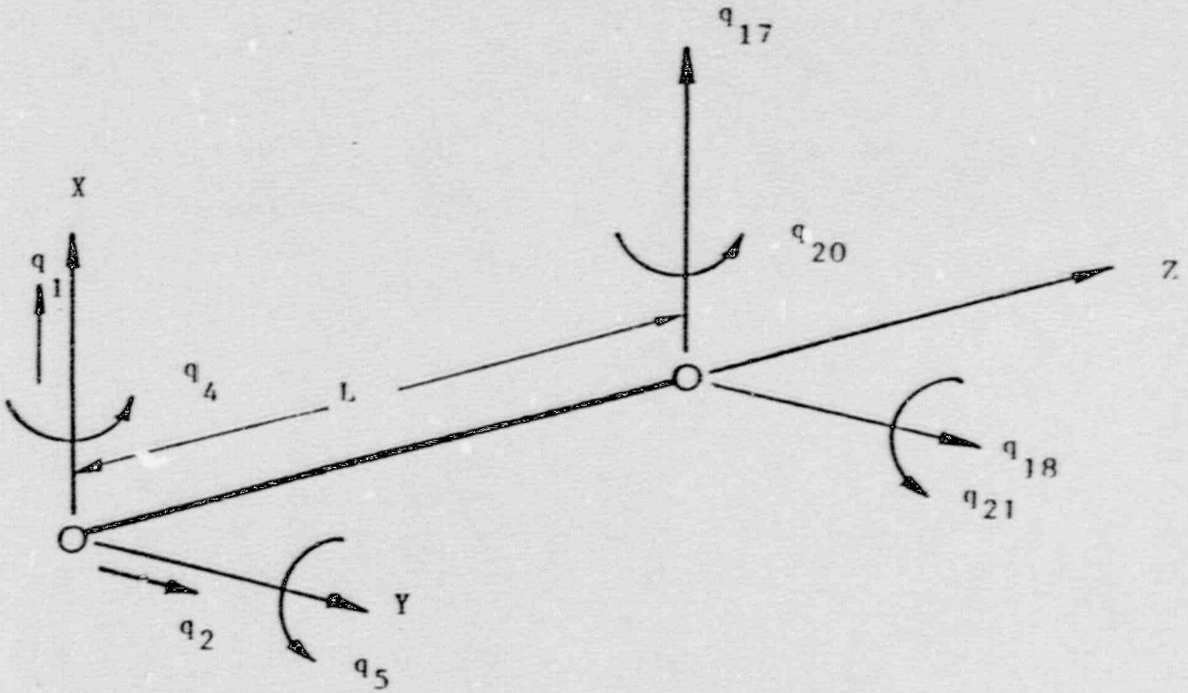

FIGURE 6.16

DEGREES OF FREEDOM MODELLING RACK MOTION

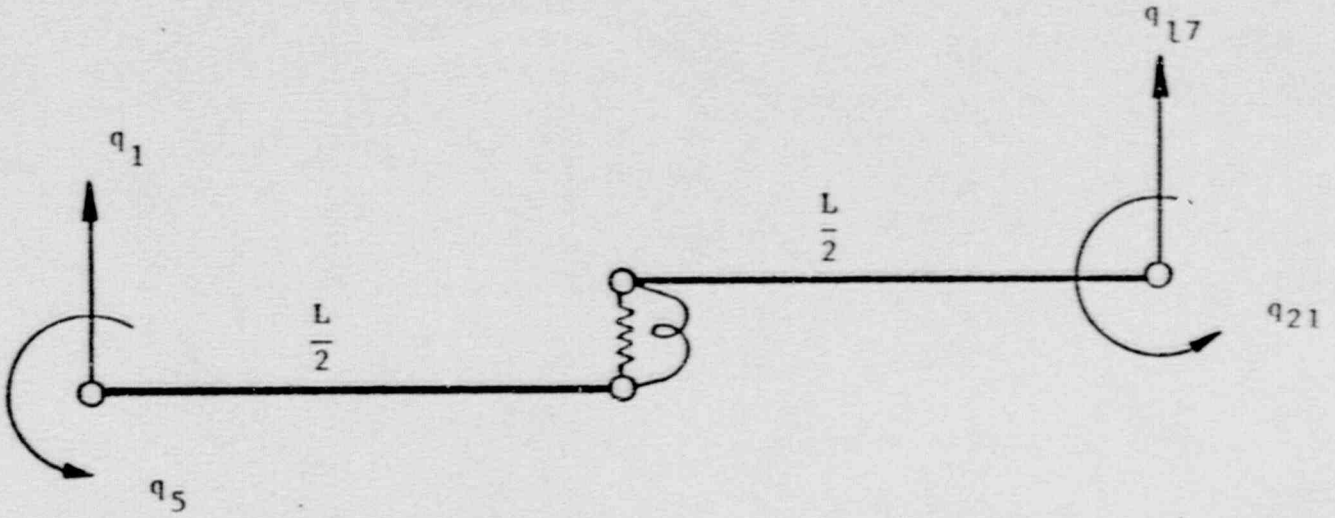

FIGURE 6.17

RACK DEGREES OF FREEDOM FOR X_Z PLANE BENDINC

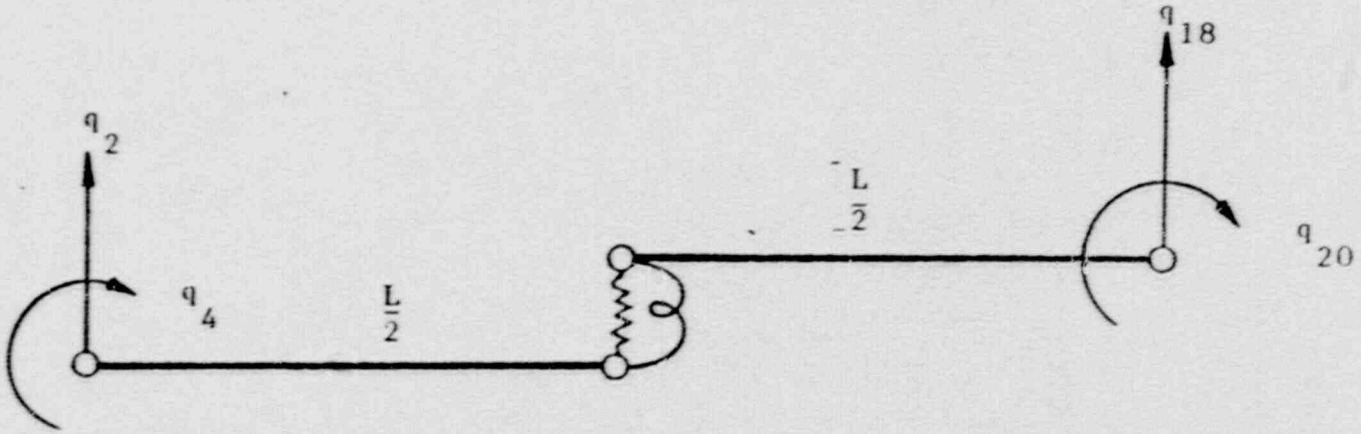

FIGURE 6.18

RACK DEGREES OF FREEDOM FOR Y-Z PLANE BENDING

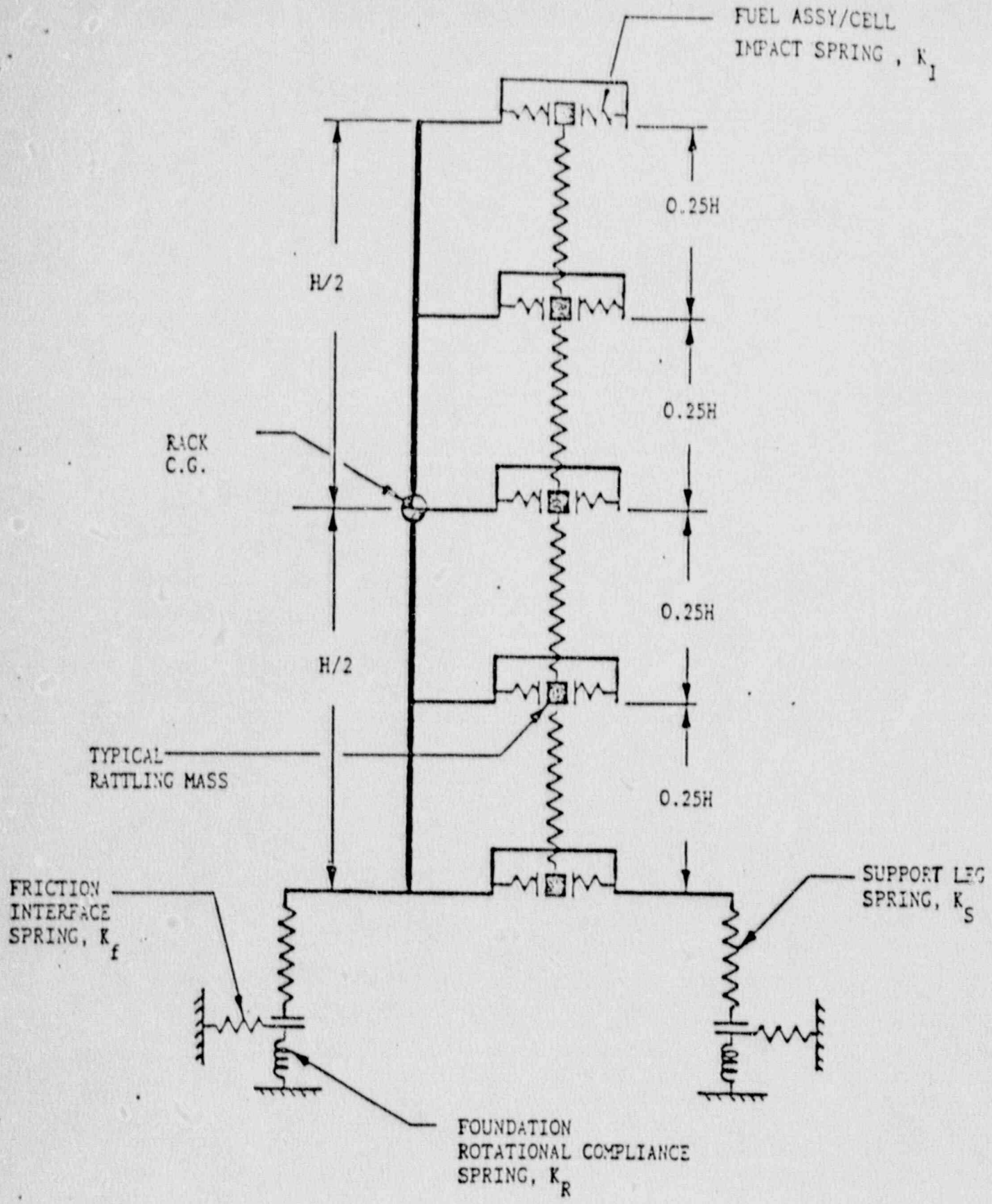

FIGURE 6.19

2-D VIEW OF RACK MODEL

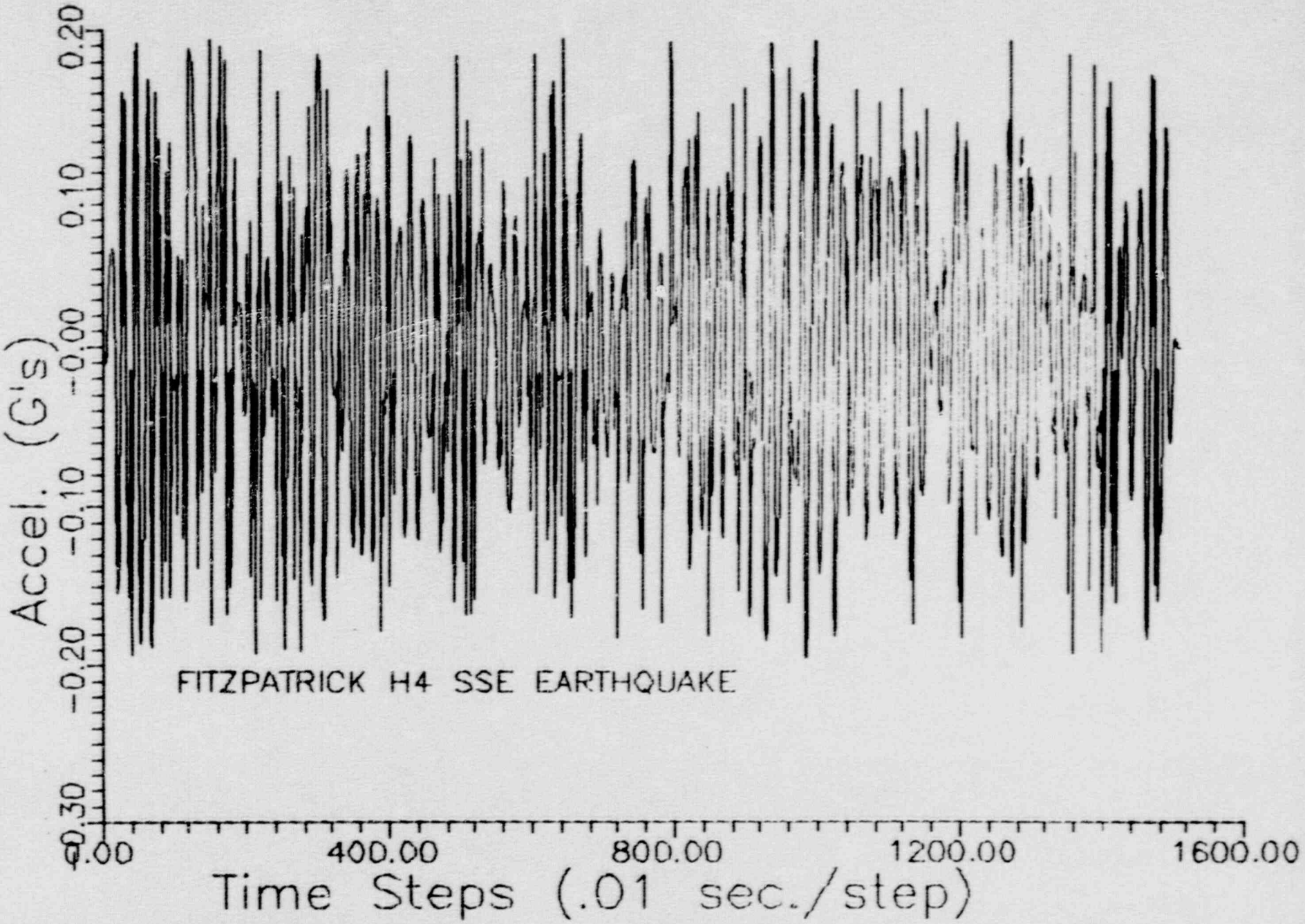
FITZPATRICK H4 SSE EARTHQUAKE
Accel. (G's)
0.20
0.10
-0.00
-0.10
-0.20
-0.30
0.00
400.00
800.00
1200.00
1600.00
Time Steps (.01 sec./step)

FIGURE 6.20

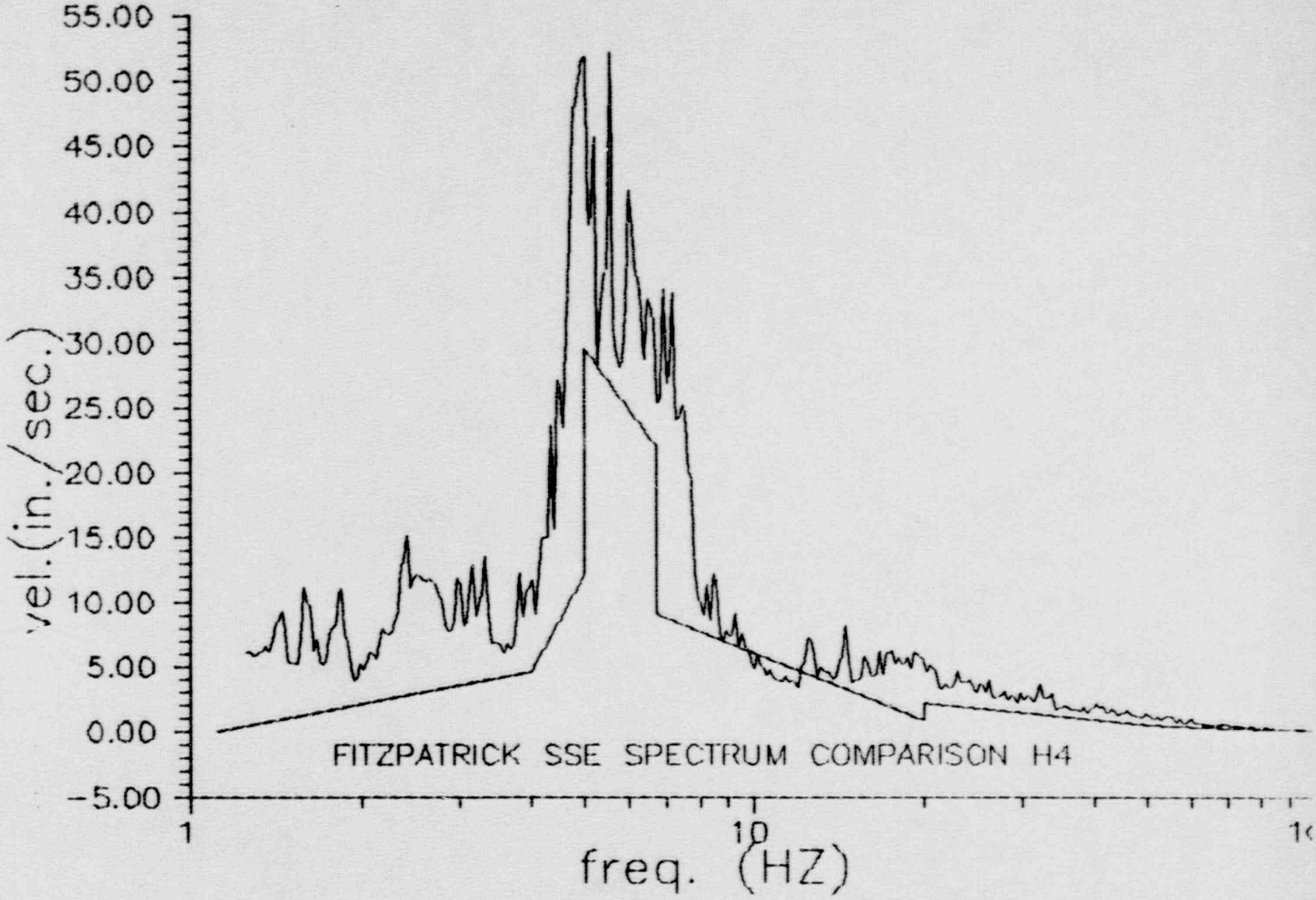
55.00
50.00
45.00
40.00
35.00
30.00
25.00
20.00
15.00
10.00
5.00
0.00
-5.00
vel.(in./sec.)
FITZPATRICK SSE SPECTRUM COMPARISON H4
1
10
freq. (HZ)

FIGURE 6.21

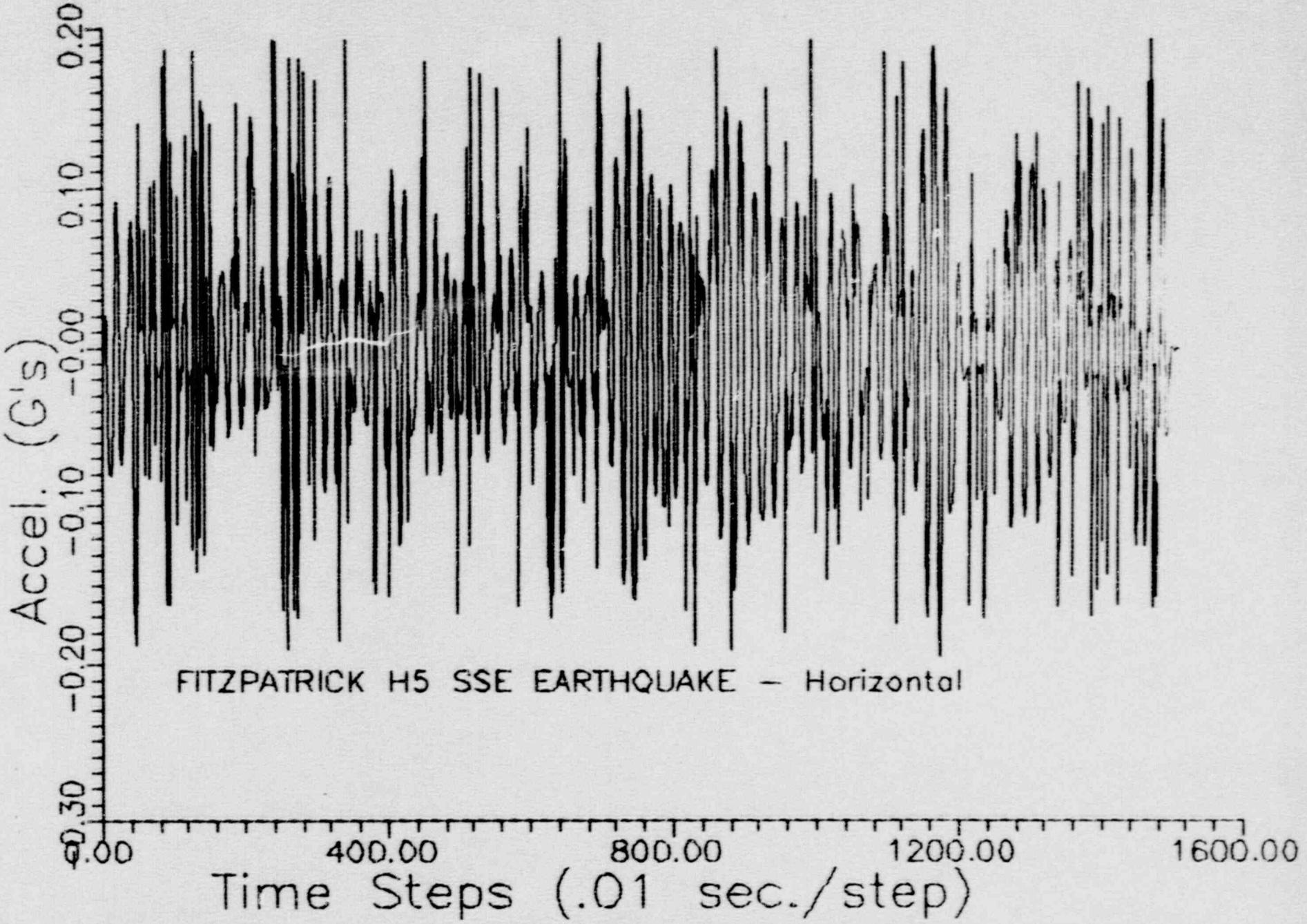
Accel. (G's)
0.20
0.10
-0.00
-0.10
-0.20
-0.30
0.00
400.00
800.00
1200.00
1600.00
Time Steps (.01 sec./step)
FITZPATRICK H5 SSE EARTHQUAKE – Horizontal

FIGURE 6.22

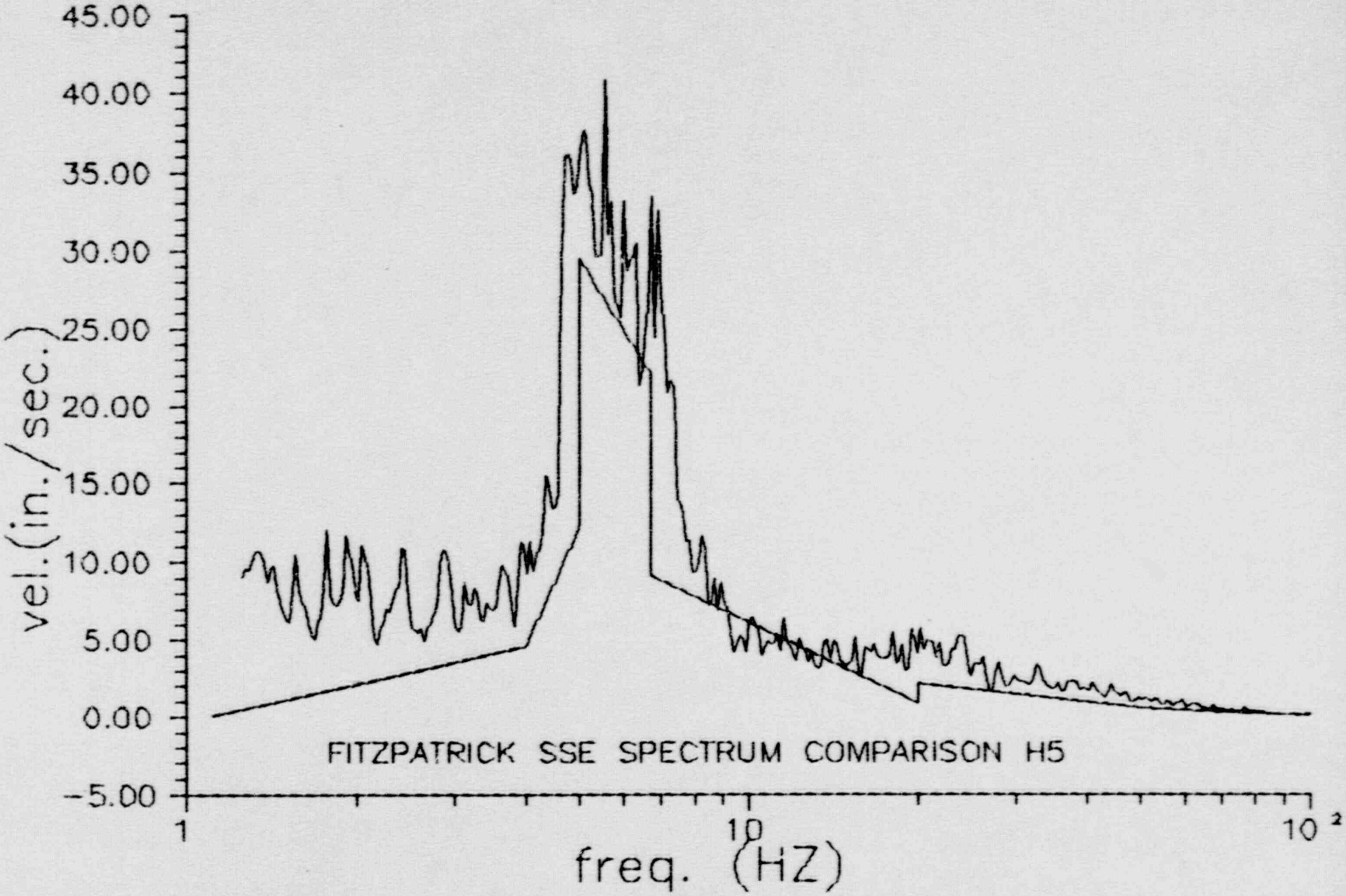
45.00
40.00
35.00
30.00
25.00
20.00
15.00
10.00
5.00
0.00
-5.00
vel.(in./sec.)
FITZPATRICK SSE SPECTRUM COMPARISON H5
1
10
10 2
freq. (HZ)

FIGURE 6.23

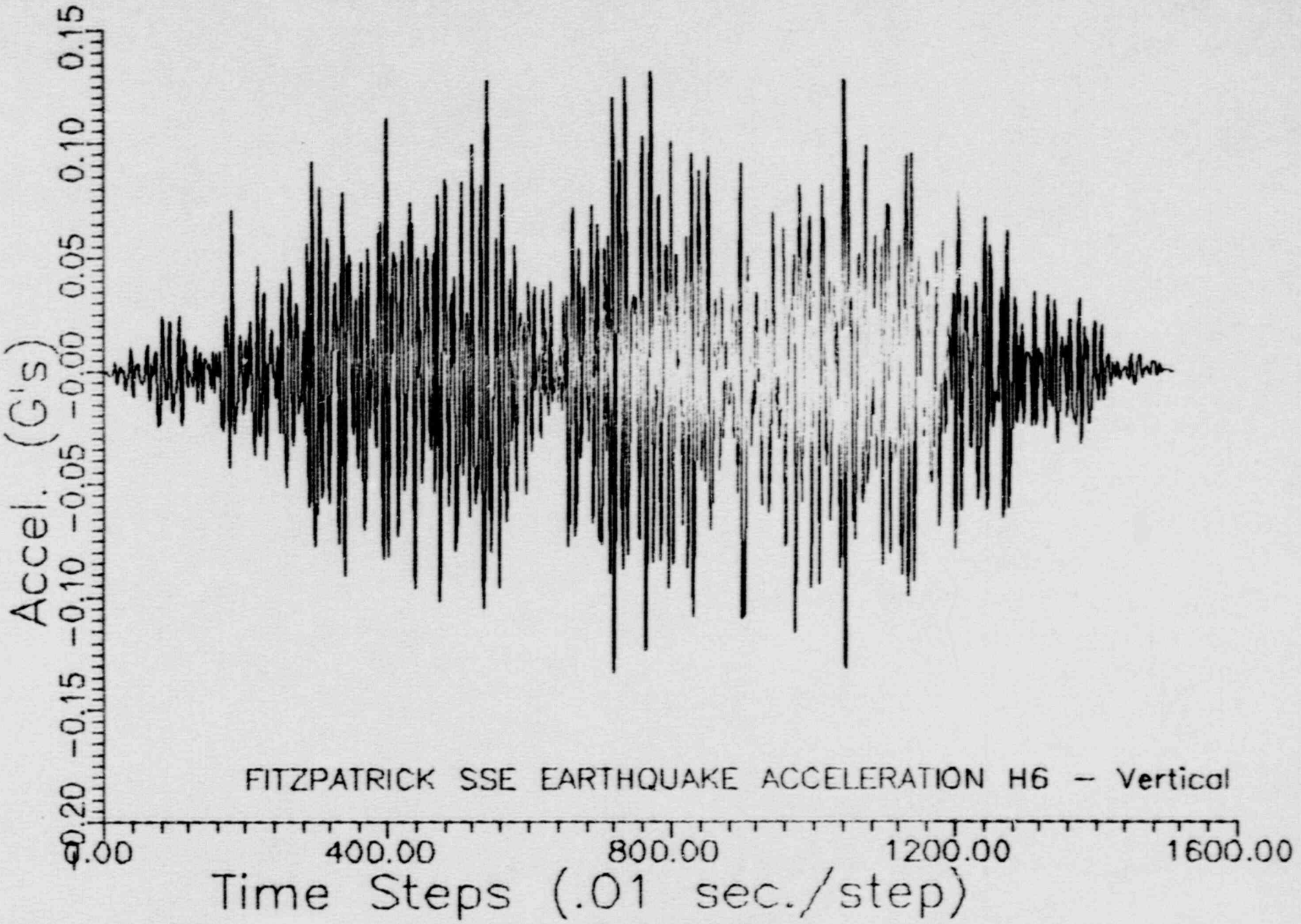
Accel. (G's)
0.15
0.10
0.05
-0.00
-0.05
-0.10
-0.15
-0.20
FITZPATRICK SSE EARTHQUAKE ACCELERATION H6 – Vertical
0.00
400.00
800.00
1200.00
1600.00
Time Steps (.01 sec./step)

FIGURE 6.24

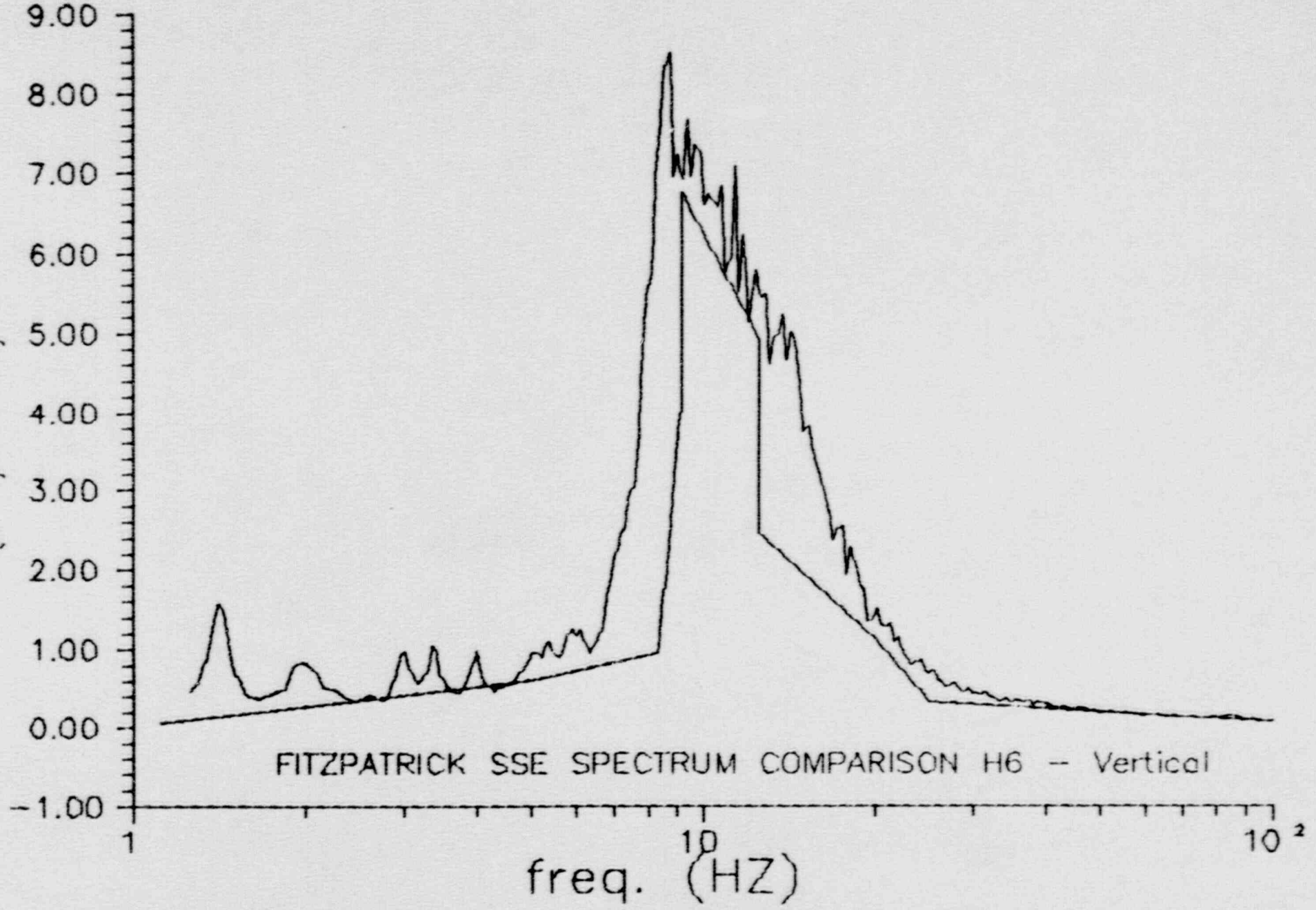
9.00
8.00
7.00
6.00
5.00
4.00
3.00
2.00
1.00
0.00
-1.00
vel.(in./sec.)
6-77
FITZPATRICK SSE SPECTRUM COMPARISON H6 -- Vertical
1
10
10 2
freq. (HZ)

FIGURE 6.25

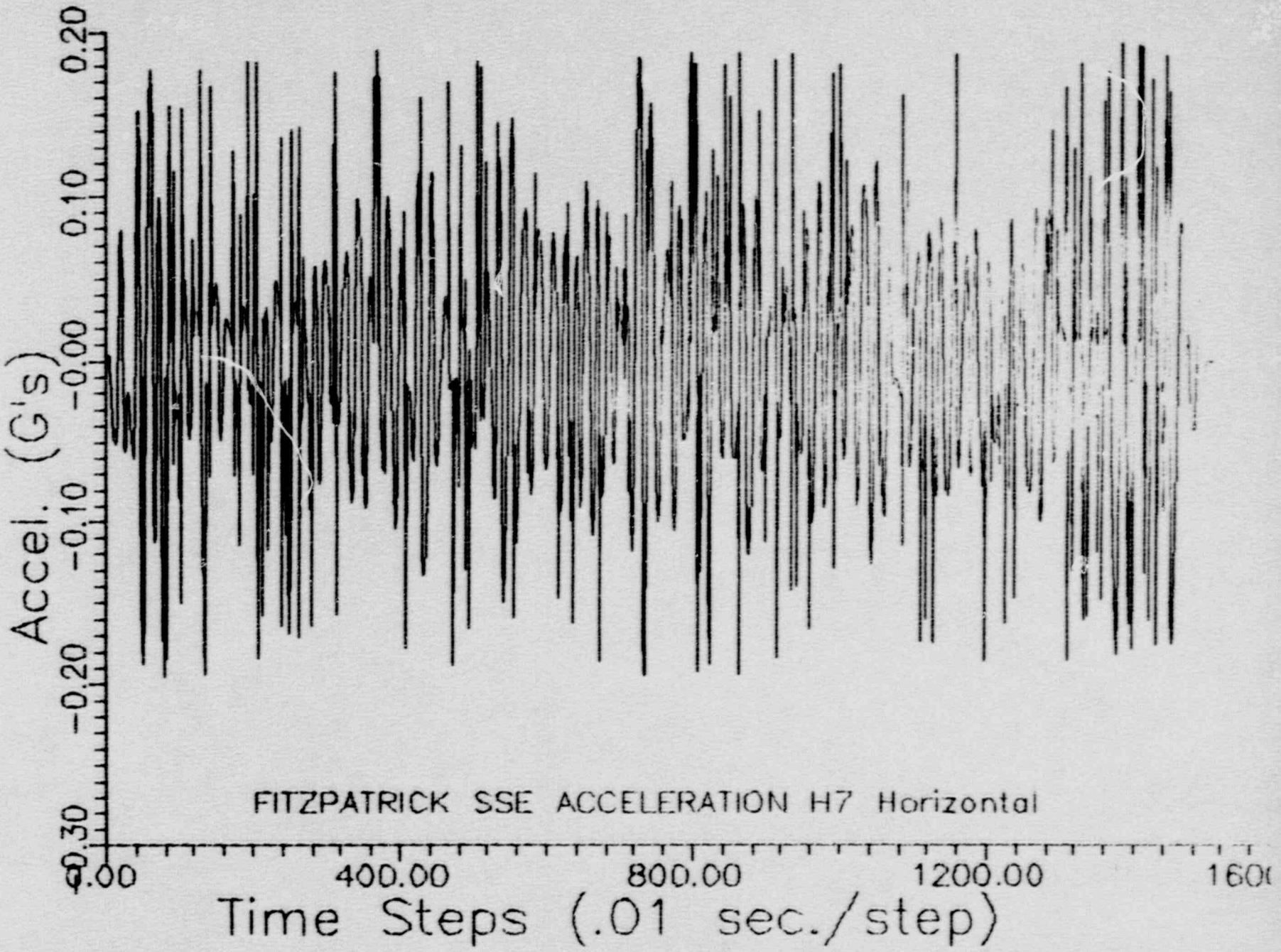
Accel. (G's)
0.20
0.10
-0.00
-0.10
-0.20
-0.30
FITZPATRICK SSE ACCELERATION H7 Horizontal
400.00
800.00
1200.00
Time Steps (.01 sec./step)

FIGURE 6.26

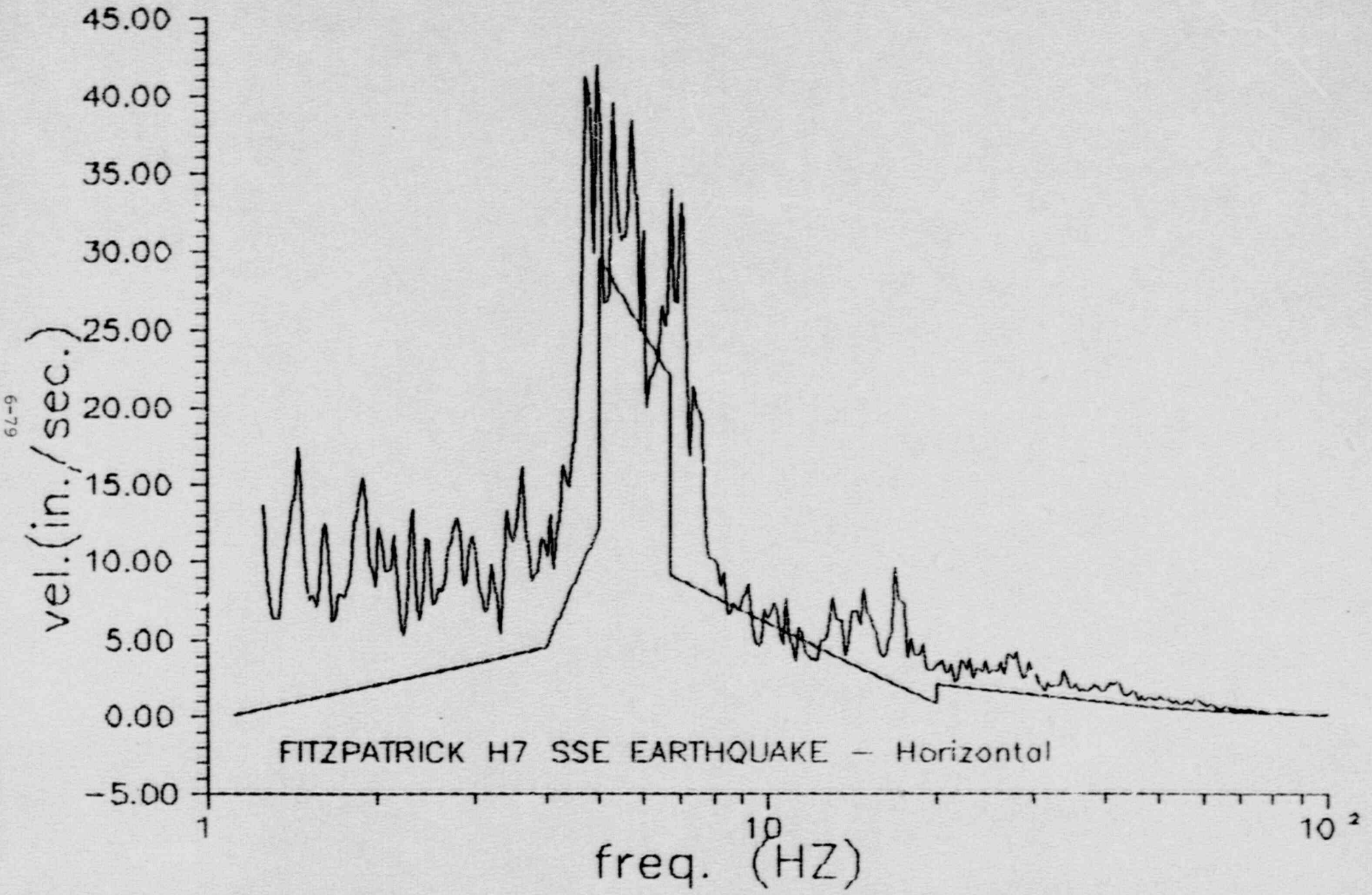
45.00
40.00
35.00
30.00
25.00
20.00
15.00
10.00
5.00
0.00
-5.00
vel.(in./sec.)
FITZPATRICK H7 SSE EARTHQUAKE – Horizontal
1
10
10 ²
freq. (HZ)

FIGURE 6.27

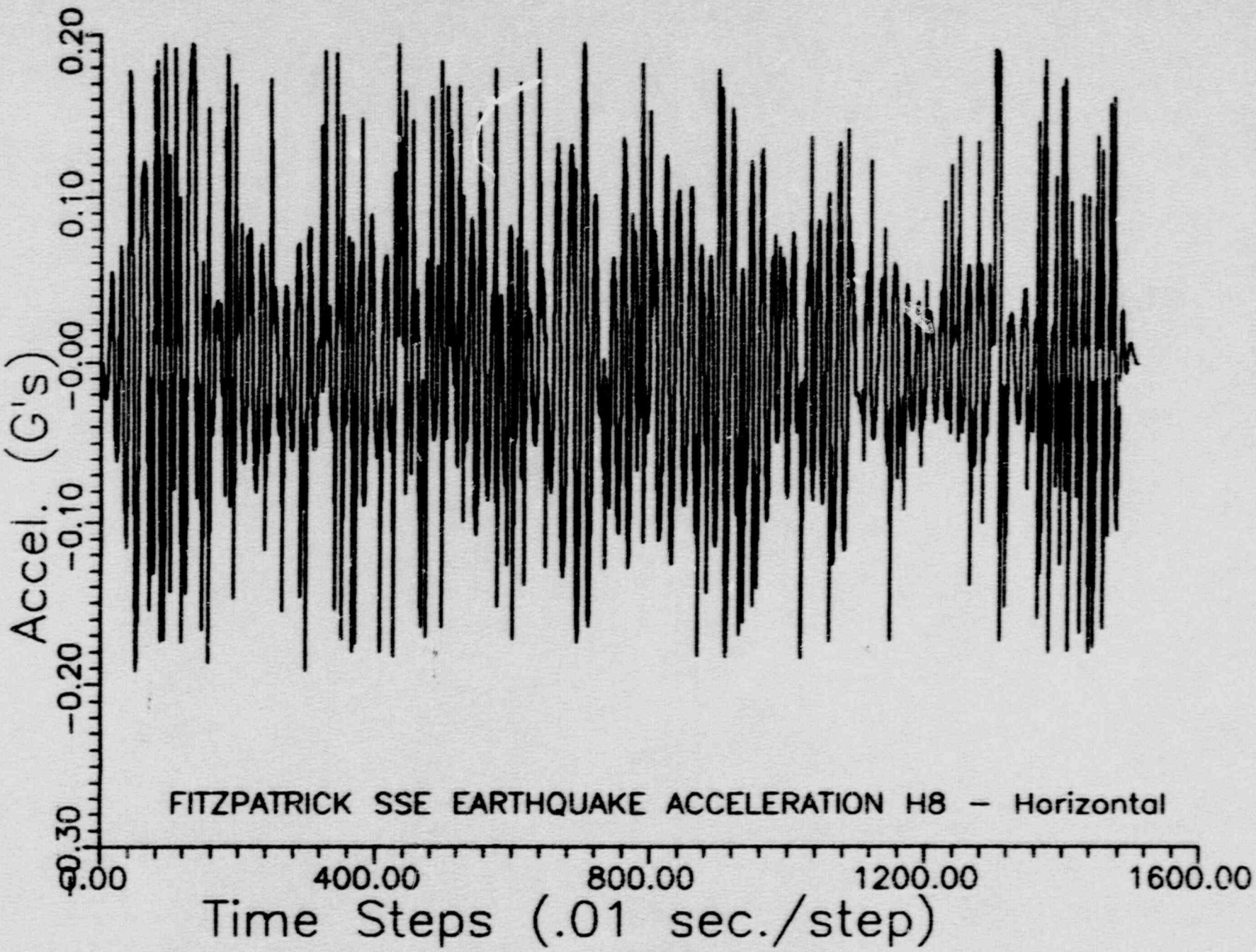
Accel. (G's)
0.20
0.10
-0.00
-0.10
-0.20
-0.30
0.00
400.00
800.00
1200.00
1600.00
Time Steps (.01 sec./step)
FITZPATRICK SSE EARTHQUAKE ACCELERATION H8 – Horizontal

FIGURE 6.28

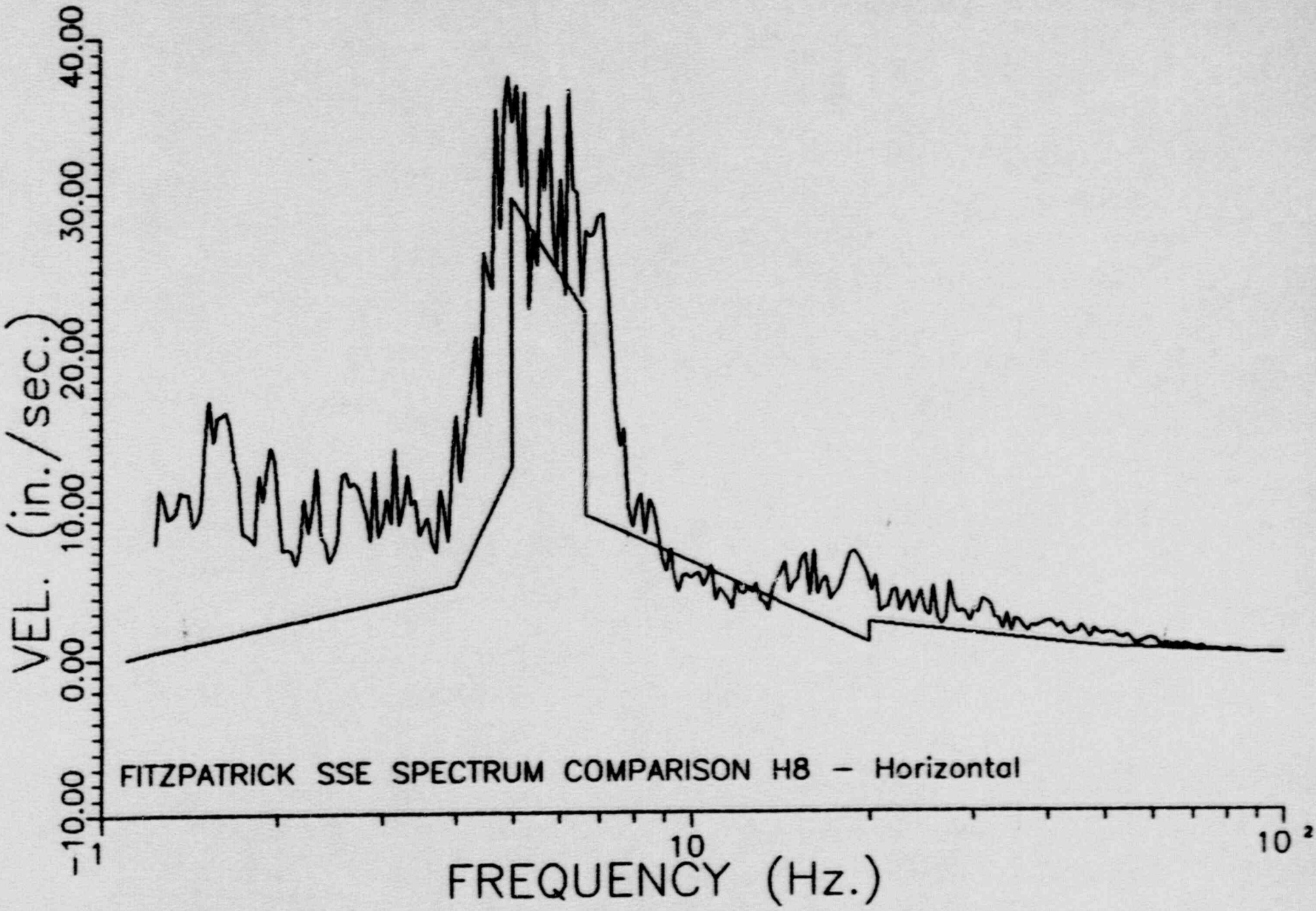
VEL. (in./sec.)
40.00
30.00
20.00
10.00
0.00
-10.00
FITZPATRICK SSE SPECTRUM COMPARISON H8 – Horizontal
10
10 ²
FREQUENCY (Hz.)

FIGURE 6.29

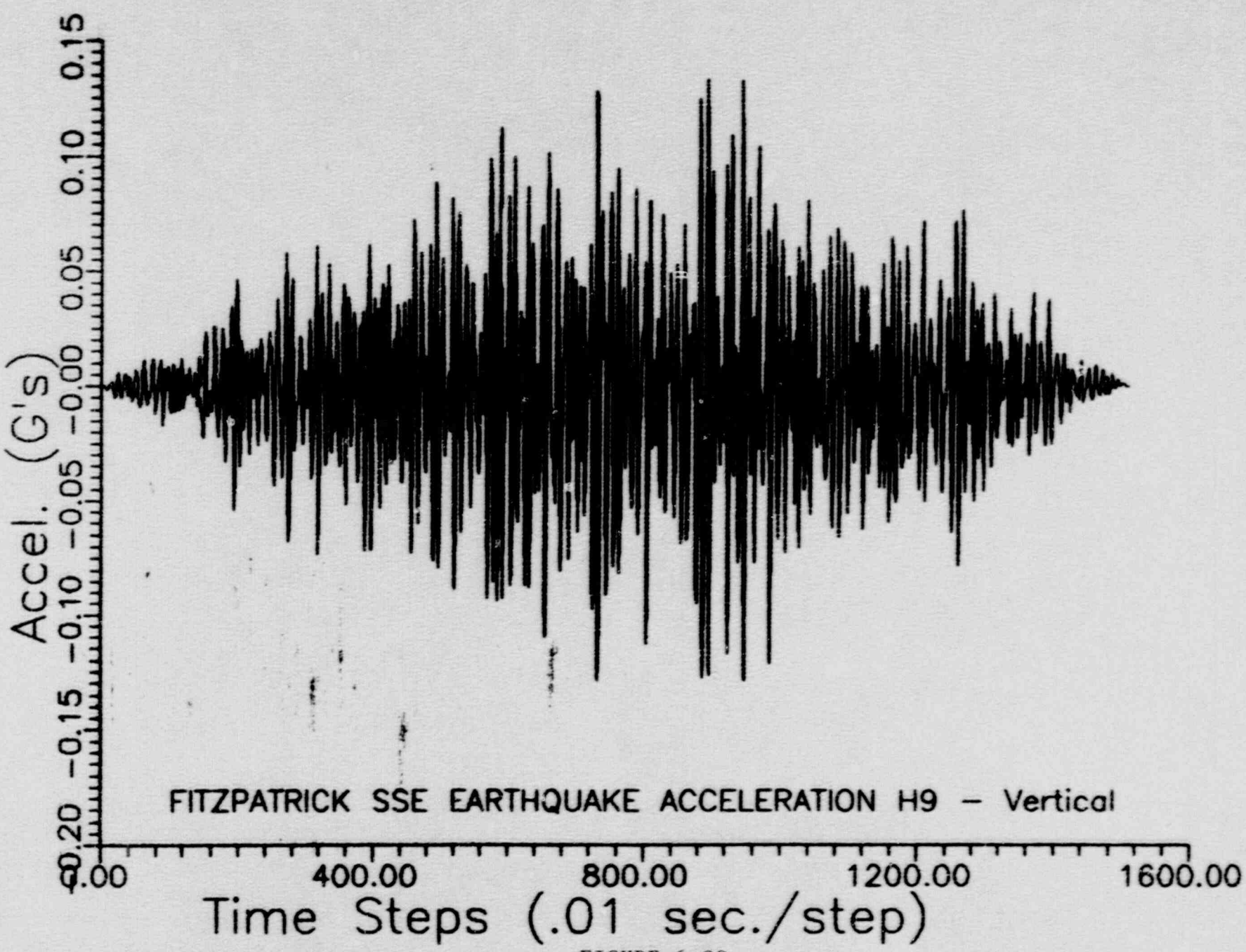
Accel. (G's)
0.20
0.15
0.10
0.05
0.00
-0.05
-0.10
-0.15
-0.20
FITZPATRICK SSE EARTHQUAKE ACCELERATION H9 – Vertical
0.00
400.00
800.00
1200.00
1600.00
Time Steps (.01 sec./step)

FIGURE 6.30

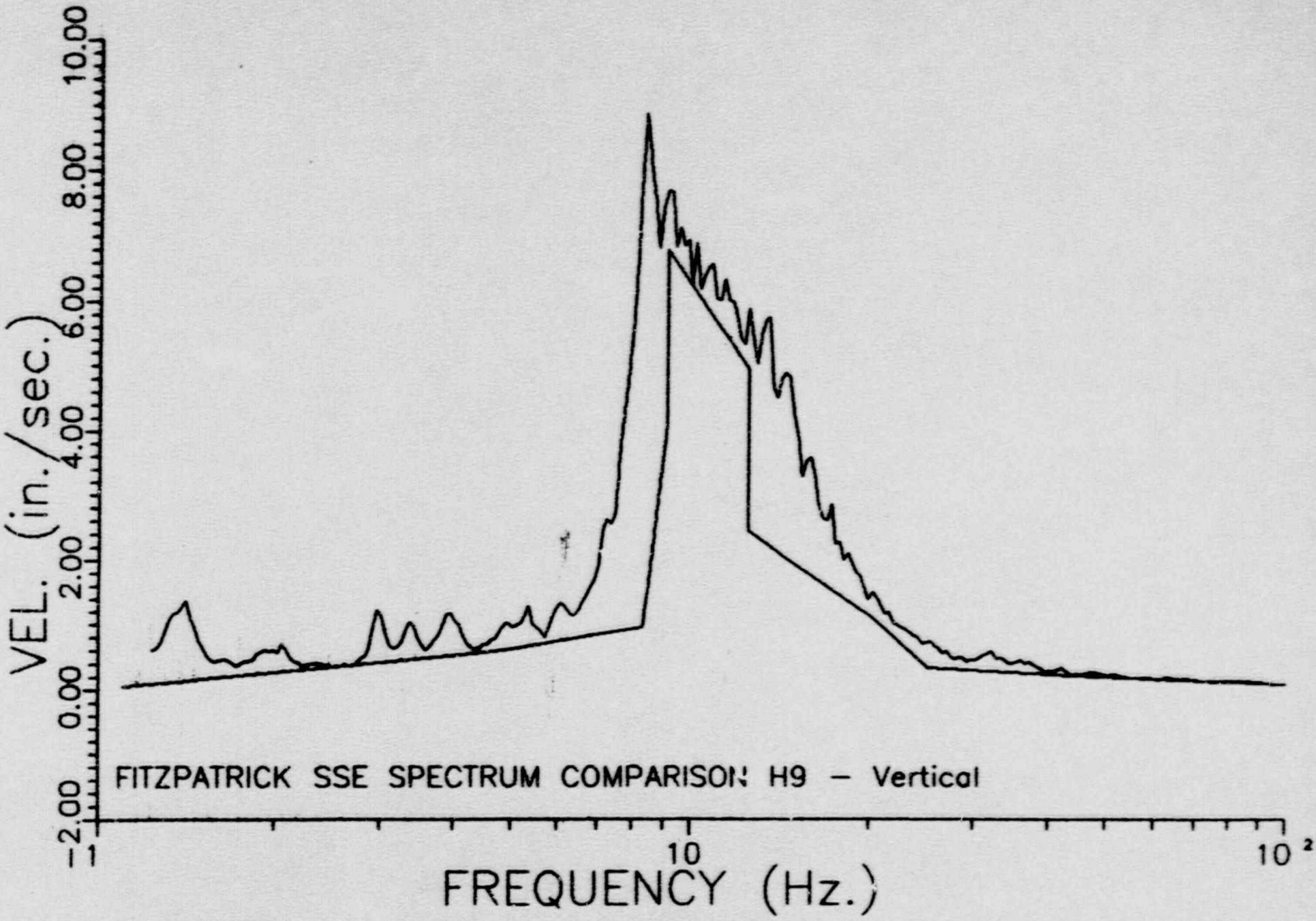
VEL. (in./sec.)
10.00
8.00
6.00
4.00
2.00
0.00
-2.00
FITZPATRICK SSE SPECTRUM COMPARISON H9 – Vertical
1
10
10 ²
FREQUENCY (Hz.)

FIGURE 6.31

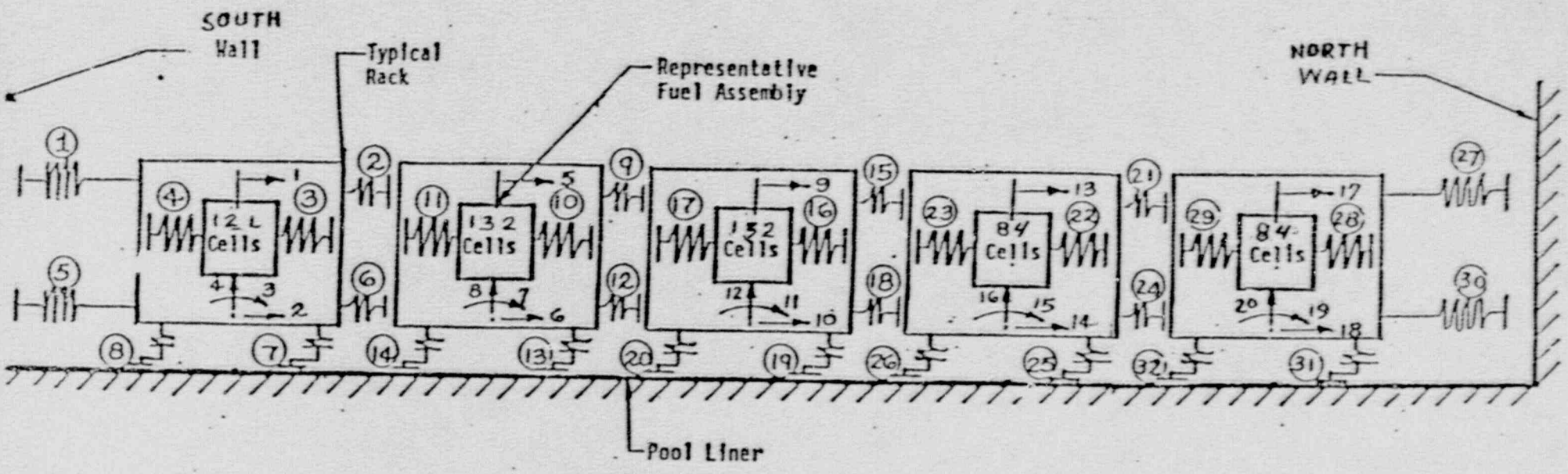

MULTI-RACK MODEL, 5 RACK ARRAY.

FIGURE 6.32

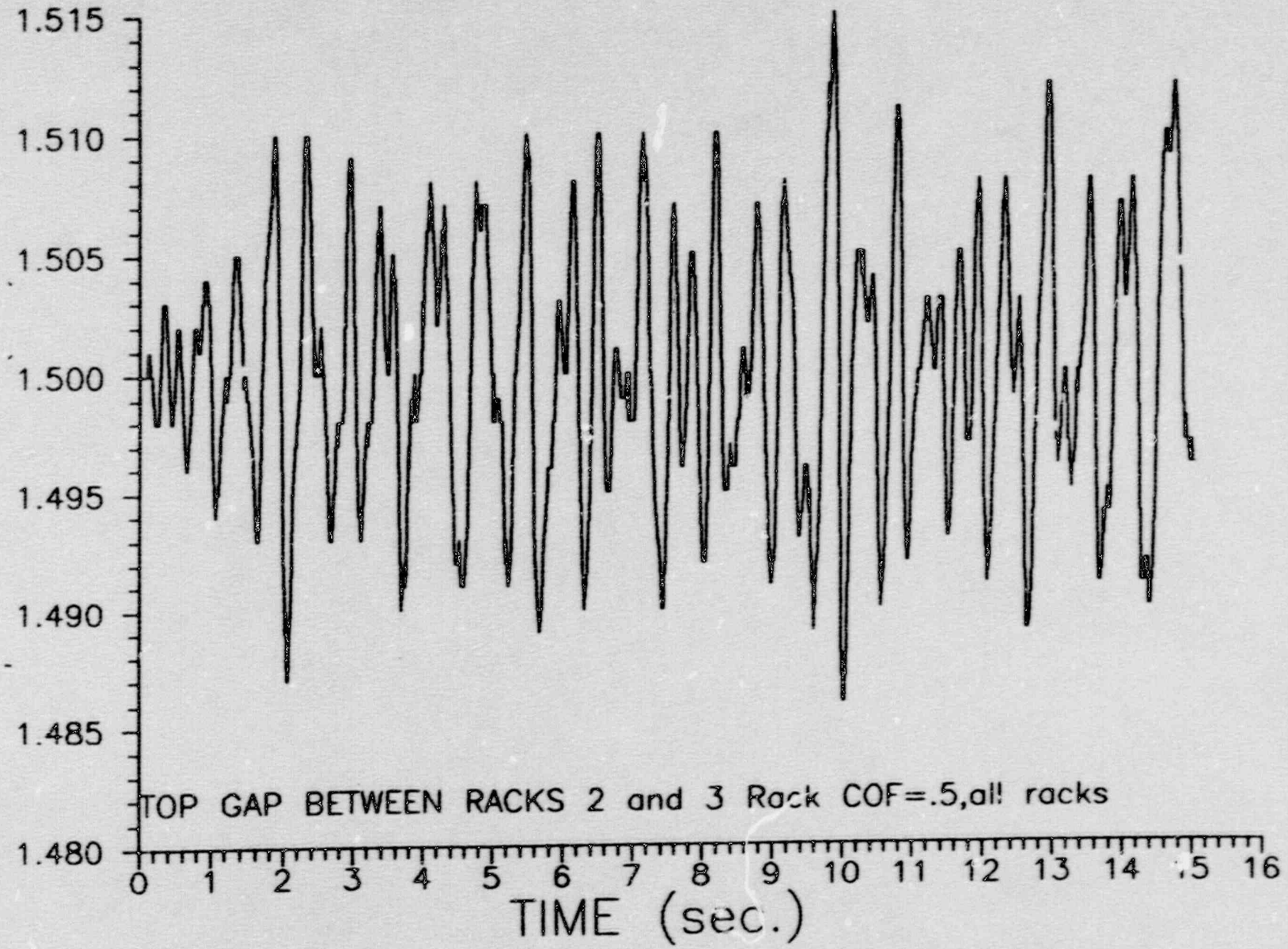
1.515
1.510
1.505
1.500
1.495
1.490
1.485
1.480
GAP SIZE (TYPICAL)
TOP GAP BETWEEN RACKS 2 and 3 Rock COF=.5,all racks
0 1 2 3 4 5 6 7 8 9 10 11 12 13 14 .5 16
TIME (sec.)

FIGURE 6.33

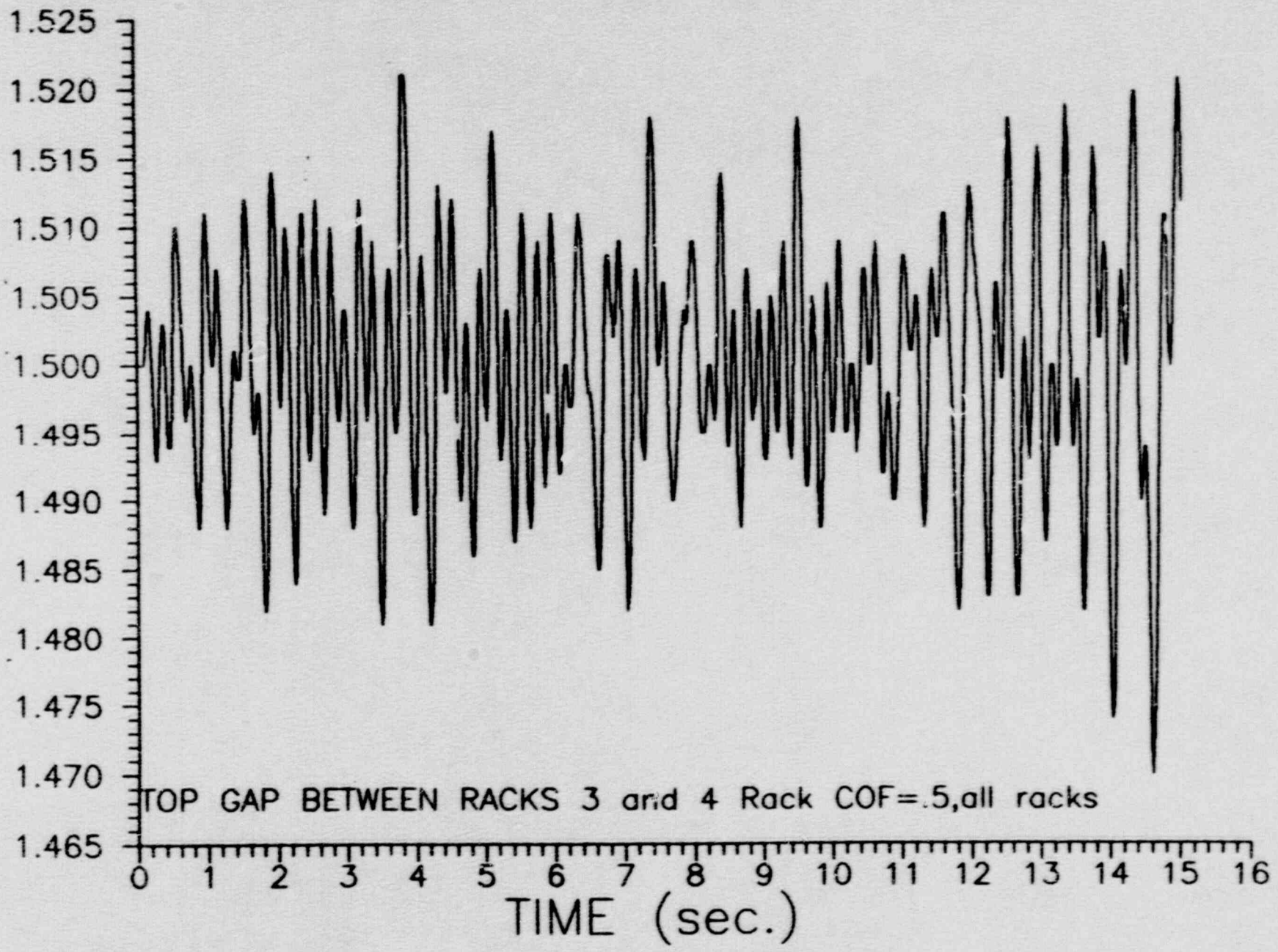
1.525
1.520
1.515
1.510
1.505
1.500
1.495
1.490
1.485
1.480
1.475
1.470
1.465
GAP SIZE (TYPICAL)
TOP GAP BETWEEN RACKS 3 and 4 Rack COF=.5,all racks
0 1 2 3 4 5 6 7 8 9 10 11 12 13 14 15 16
TIME (sec.)
98-9

FIGURE 6.34

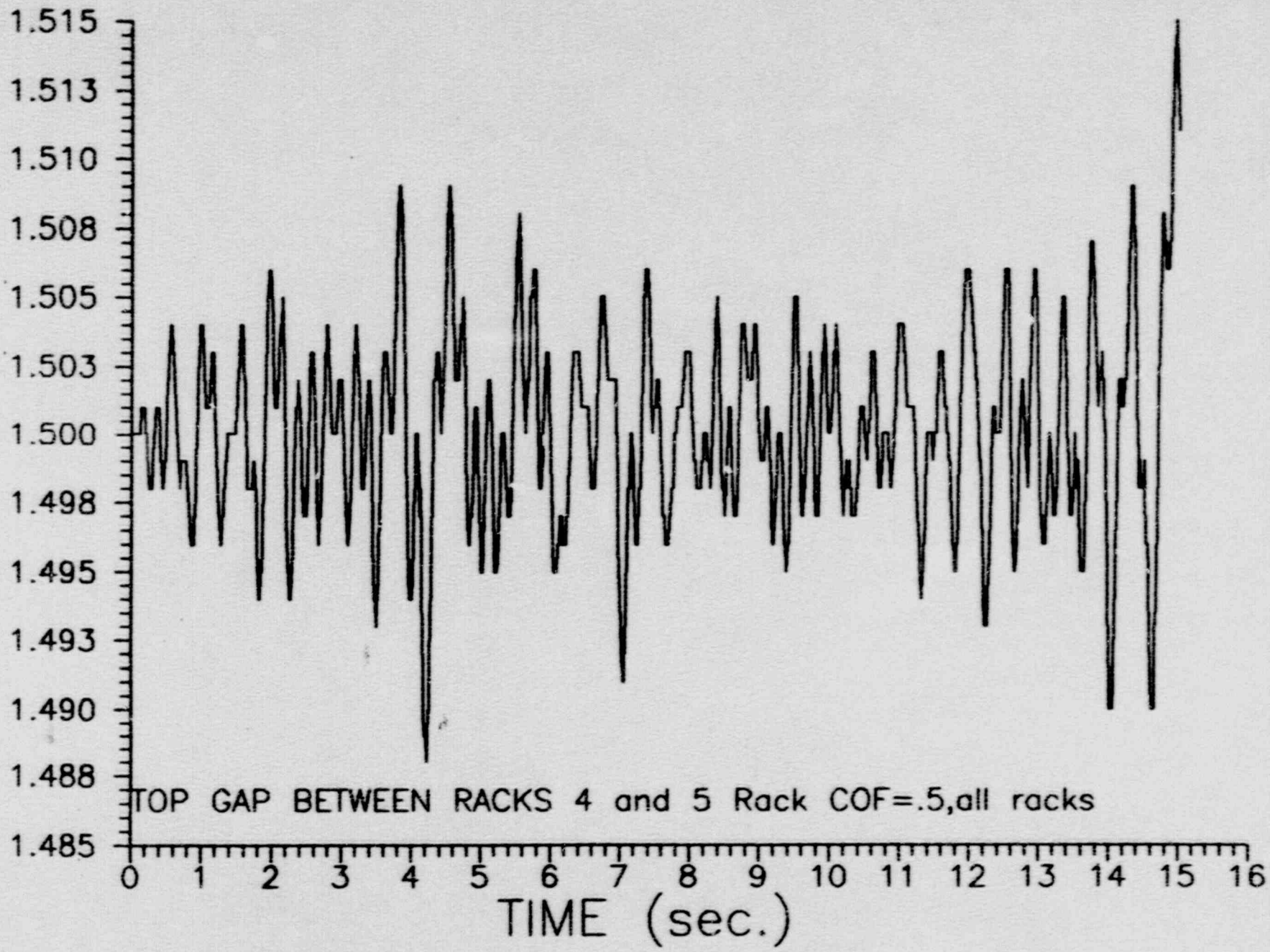
1.515
1.513
1.510
1.508
1.505
1.503
1.500
1.498
1.495
1.493
1.490
1.488
1.485
GAP SIZE (TYPICAL)
TOP GAP BETWEEN RACKS 4 and 5 Rack COF=.5,all racks
0 1 2 3 4 5 6 7 8 9 10 11 12 13 14 15 16
TIME (sec.)

FIGURE 6.35

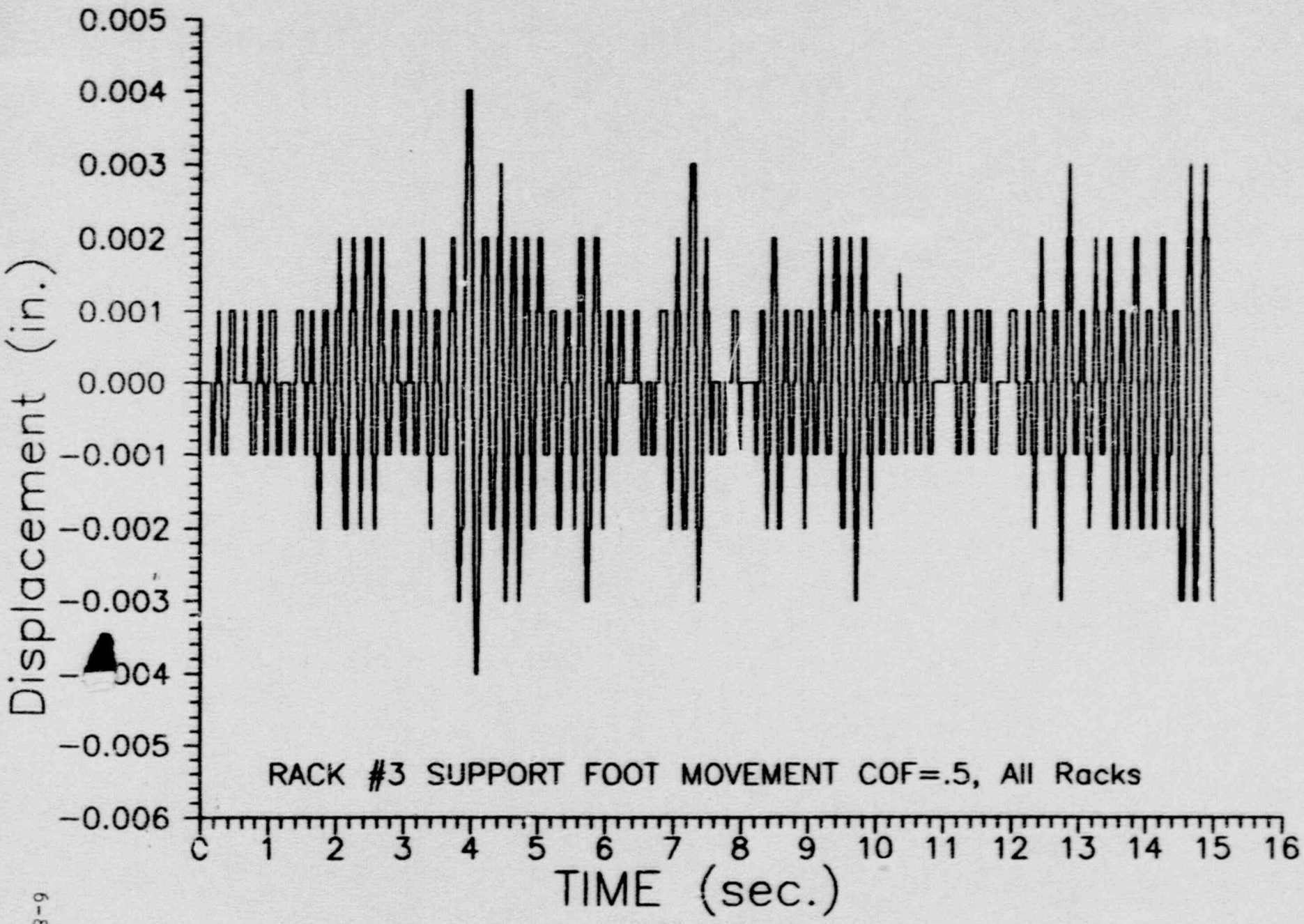

88-9

FIGURE 6.36